Biodistribution of surfactant-free poly(lactic-acid) nanoparticles and uptake by endothelial cells and phagocytes in zebrafish: Evidence for endothelium to macrophage transfer.

Julien Rességuier, Jean-Pierre Levraud, Nils Dal, Federico Fenaroli, Charlotte Primard, Jens Wohlmann, Gabrielle Carron, Gareth Griffiths, Dominique Le Guellec, Bernard Verrier

Journal of Controlled Release 331 (2021) 228–245

Contents lists available at ScienceDirect

Journal of Controlled Release

journal homepage: www.elsevier.com/locate/jconrel

Biodistribution of surfactant-free poly(lactic-acid) nanoparticles and uptake by endothelial cells and phagocytes in zebrafish: Evidence for endothelium to macrophage transfer.

Julien Rességuier [a,b,*], Jean-Pierre Levraud [c,1], Nils K. Dal [b,1], Federico Fenaroli [b], Charlotte Primard [d], Jens Wohlmann [b], Gabrielle Carron [a], Gareth W. Griffiths [b], Dominique Le Guellec [a], Bernard Verrier [a]

[a] CNRS, University Lyon 1, UMR 5305, Laboratory of Tissue Biology and Therapeutic Engineering, IBCP, 7 Passage du Vercors, 69367 Lyon Cedex 07, France
[b] Department of Biosciences, University of Oslo, Blindernveien 31, 0371 Oslo, Norway
[c] Macrophages et Développement de l'Immunité, Institut Pasteur, CNRS UMR3738, 75015 Paris, France
[d] Adjuvatis, 7 Passage du Vercors, 69007 Lyon, France

ARTICLE INFO

Keywords:
Surfactant-free
Biodistribution
Nanoparticles
Zebrafish
Uptake-degradation kinetics
Endothelial cell to macrophage transfer

ABSTRACT

In the development of therapeutic nanoparticles (NP), there is a large gap between *in vitro* testing and *in vivo* experimentation. Despite its prominence as a model, the mouse shows severe limitations for imaging NP and the cells with which they interact. Recently, the transparent zebrafish larva, which is well suited for high-resolution live-imaging, has emerged as a powerful alternative model to investigate the *in vivo* behavior of NP. Poly(D,L lactic acid) (PLA) is widely accepted as a safe polymer to prepare therapeutic NP. However, to prevent aggregation, many NP require surfactants, which may have undesirable biological effects. Here, we evaluate 'safe-by-design', surfactant-free PLA-NP that were injected intravenously into zebrafish larvae. Interaction of fluorescent NPs with different cell types labelled in reporter animals could be followed in real-time at high resolution; furthermore, by encapsulating colloidal gold into the matrix of PLA-NP we could follow their fate in more detail by electron microscopy, from uptake to degradation. The rapid clearance of fluorescent PLA-NP from the circulation coincided with internalization by endothelial cells lining the whole vasculature and macrophages. After 30 min, when no NP remained in circulation, we observed that macrophages continued to internalize significant amounts of NP. More detailed video-imaging revealed a new mechanism of NP transfer where NP are transmitted along with parts of the cytoplasm from endothelial cells to macrophages.

1. Introduction

Since their introduction in the 1960s', a wide variety of nanoparticles (NP) have been developed, although only a few of them have been clinically approved [1]. It can be argued that a major factor contributing to this situation has been the large gap that has formed between *in vitro* testing and *in vivo* experimentation during the development of NP. Accordingly, the common strategy is to test NP at the level of cell culture and to select the most promising formulations for their behavior in an appropriate mouse model, in which the NP can at best be seen only at low resolution, unless one uses invasive methods. This jump from cells to mouse hinders our understanding of the biological interactions of NP, especially at the tissue and cellular level, which would provide helpful hindsight to optimize the design of NP and their use for therapeutic applications.

The success of NP also depends on the choice of scaffold material used to assemble the NP, most commonly polymer-based ones. Widely used polymers are part of the aliphatic family, including Poly Lactic-*co*-Glycolic Acid (PLGA) and Poly Lactic Acid, both materials that are FDA-approved for clinical use. However, in most cases the assembly of non-aggregated NP requires the use of a surfactant, such as Polyvinylpyrrolidone (PVP) or Polyvinyl alcohol (PVA), to reduce the surface tension of the NP and to stabilize them [2]. These surfactants may have undesirable side-effects [3–6] and our group has put significant effort in

* Corresponding author at: CNRS, University of Lyon 1 - UMR5305 / University of Oslo, Department of Biosciences, Norway.
E-mail address: julien.resseguier@ibv.uio.no (J. Rességuier).
[1] Both authors equally contributed to the research article.

https://doi.org/10.1016/j.jconrel.2021.01.006
Received 19 June 2020; Received in revised form 16 November 2020; Accepted 4 January 2021
Available online 11 January 2021

preparing safe-by-design PLA-NP without surfactants and with levels of residual solvent that are in agreement with the European pharmacopeia for human use [7,8]; this idea also fits well with general recommendations to simplify the procedures for making NP [9,10]. Both vaccine [11] and mRNA-vectorization [12] applications have been successfully made and characterized with such PLA-NP. However, like other safe-by-design or surfactant-free NP system, their biological interactions and fate after administration remain poorly understood.

The zebrafish larva is a vertebrate model with the great advantage of being highly transparent, thereby allowing researchers to analyze the biodistribution of NPs at high resolution in real time and in a non-invasive manner [13,14]. Moreover, genetically modified fish are available that selectively express different colored fluorescent proteins in specific cell types. Altogether, the zebrafish model emerges as a reliable intermediary model to bridge *in vitro* experimentation and *in vivo* experimentation in higher vertebrate. In a previous study, we have exploited this powerful system to analyze the uptake of PLA-NP by mucosal surfaces [15]. In this work, we monitored the uptake and fate of safe-by-design, surfactant-free PLA-NPs after intravenous injection. PLA-NPs were cleared from the blood in less than 30 min, and took several days to disassemble. We identify endothelial cells and macrophages as the two cell populations that internalize PLA-NPs, and describe the unexpected transfer of PLA-NPs, along with some cytoplasmic material, from vascular endothelial cells to macrophages.

2. Results

2.1. Characterization of safe-by-design fluorescent PLA-NP

Following a safe-by design strategy to produce nanocarriers as simply as possible, but having high biocompatibility, Poly(D,L lactic acid) particles, were prepared by nanoprecipitation without the addition of surfactant or stabilizer. During this process, the small length of the PLA (<50,000 g/mol) chains enables enough negatively charged carboxyl groups to be exposed at the surface of the PLA-NP, ensuring colloidal stabilization [16]. Importantly, residual solvents (water and acetone) were gently evaporated until their minimal concentration respected the standards established by the European pharmacopeia for human use, as assessed by gas chromatography quantification (data not shown). The visualization of PLA-NP formulations was made possible by the encapsulation of different hydrophobic fluorophores into the polymeric matrix. As measured by dynamic light scattering (DLS), we obtained highly homogeneous (Polydispersity index < 0.05) suspensions of red, green and far-red fluorescent PLA-NP which displayed *Z*-average of 174 nm ± 7 nm (mean(SD)), and strong anionic zeta potentials around −55 mV (Table 1). Throughout our experiments, we injected 3–5 nL of PLA-NP at 5 mg/mL in 3 day post-fertilization (dpf) zebrafish larvae. Since a larva weighs ~ 0.4 mg, this translates to approximatively 50 mg/kg. At this high dose, neither development nor health of injected larvae were visibly impaired by the injection of our fluorescent PLA-NP, reflecting their great biocompatibility.

2.2. Internalization of PLA-NP by endothelial cells from the whole vasculature

Despite their promising potential for nanomedicine, very few studies have been conducted to characterize the fate of surfactant-free NP *in vivo*. Following standard protocols [13,17], fluorescent PLA-NP (5 mg/mL) were intravenously injected into 3 dpf zebrafish, through either the post-cardinal vein or the inferior segment of the caudal vein plexus (Fig. S1). Our initial investigation of the PLA-NP biodistribution was performed by live-imaging, using an epi-fluorescent stereomicroscope, on transgenic fli1a:GFP fish [18], where endothelial cells express a green fluorescent protein in their cytoplasm. Note that in this transgenic line, neural crest cells and some macrophage progenitors can also express GFP.

Two hours following intravenous injection, red fluorescent PLA-NP were observed along the whole vasculature, from the tail region to the heart, brain and ocular vessels (Fig. 1: A). Furthermore, the fluorescence from PLA-NP seemed in close association with the fluorescence of endothelial cells, suggesting possible interactions with these cells (Fig. 1: A'-A"– Yellow arrowheads). To better visualize these potential interactions, we performed high-resolution 3D live-imaging using a high-speed spinning-disk confocal microscope, which minimizes phototoxicity. We observed extensive internalization of PLA-NP by the endothelial cells. Massive clusters of fluorescence from PLA-NP were especially found in those endothelial cells forming the caudal vein plexus (Fig. 1: B-B″). In addition, less striking uptake was seen into the endothelial cells lining the caudal artery and intersegmental vessels (Fig. 1: C).

Analysis of the optical sections revealed that PLA-NP internalized by endothelial cells were contained within large intracellular compartments devoid of GFP and not within the GFP labelled cytosol (Fig. 1: B″ - lower blue panel). In addition, the fluorescence from free-circulating PLA-NP could not be detected within the bloodstream, nor at the plasma membrane surface of endothelial cells. However, large accumulations of PLA-NP were also detected in presumed phagocytes residing in the lumen of blood vessels. Intriguingly, it appeared that some of these phagocytes internalized both PLA-NP and GFP-labelled material (Fig. 1: B″ - upper white panel). A 3D reconstruction of the acquired image is presented in (Video S1).

Experiments in zebrafish embryos have shown essentially exclusive binding and internalization of different anionic NP to scavenger-endothelial cell in restricted venous sites, namely the caudal vein plexus and the dorsal aspect of the post-cardinal vein [19–22]. This uptake process was shown to be dependent on the scavenger receptor Stab2. In contrast, cationic NP were internalized by endothelial cells throughout the vasculature, independently of Stab2. In agreement with the above studies our anionic PLA-NP were massively internalized by endothelial cells that form the caudal vein plexus. Surprisingly however, our NP were also taken up by venous and arterial endothelial cells lining the entire system. Examples of localizations in the dorsal aorta, intersegmental vessels and both dorsal and ventral aspects of the post-cardinal vein are evident in (Fig. 1: C); uptake into the dorsal

Table 1
Fluorescent NP characteristics.

Name	Fluorophore / PHR*	Diameter	PdI	Zeta potential	Fish survival at 24 h post injection
PLA-BODIPY TR	Bodipy TR methyl ester / 0.02 %	182 nm	0.019	-52.8 mV	100 %
PLA-BODIPY FL	Bodipy 500-510 $_{C4,C9}$ / 0.04 %	171 nm	0.024	-57.1 mV	100 %
PLA-DY650	DY650-decylamide / 0.10 %	170 nm	0.018	-56.9 mV	100 %

* parts per hundred of resin

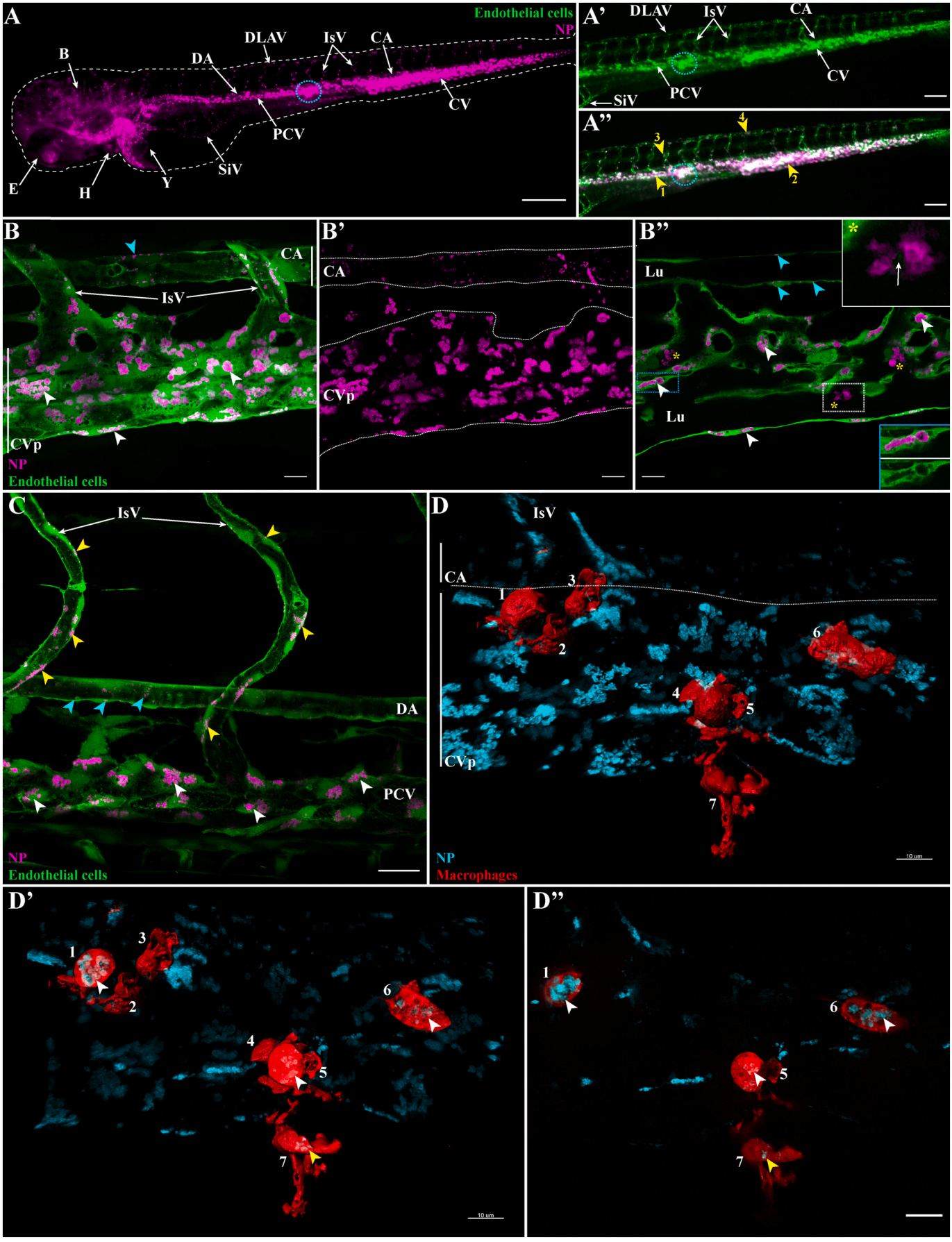

(caption on next page)

Fig. 1. Internalization of PLA-NP by endothelial cells and macrophages. Representative live-acquisitions of 3 dpf zebrafish, 2 h after intravenous administration of PLA-NP, using a stereomicroscope (A-A") or a spinning-disk confocal microscope (B-D"). (A-A") Fluorescent PLA-NP (magenta) appear closely associated (yellow arrows) with the whole vasculature of fli:GFP^{+} fish (green). Injection sites are usually at the post-cardinal veins (blue circle) or within the inferior region of the caudal vein. As illustrated by the maximum intensity projection (MIP), which displays both PLA-NP and endothelial cells (B) and PLA-NP only (B′), strong accumulations of PLA-NP are observed within the endothelial cells of the caudal vein plexus (white arrowheads). PLA-NP are also taken-up by the endothelial cells of the caudal artery (cyan arrowheads). (B″) As revealed by optical sections (B), among both the caudal vein plexus and the caudal artery (white and cyan arrowheads, respectively), PLA-NP within endothelial cells are stored inside GFP negative cellular compartments. This localization is even more striking when the fluorescence signal from PLA-NP is removed (blue panel). Cluster of PLA-NP could be observed among luminal phagocytes (yellow stars). Co-internalization of GFP and PLA-NP within some luminal phagocytes has also been noticed (white arrow within white panel). (C) PLA-NP internalization is not restricted to the caudal vein plexus or the dorsal aspect of the post-cardinal vein. Endothelial cells from the whole post-cardinal vein (white arrowhead), the intersegmental vessels (yellow arrowhead) and the dorsal aorta (cyan arrowhead) are PLA-NP-positive, illustrating the pan-vascular internalization of PLA-NP. (D) From a mpeg1:mCherry zebrafish, MIP illustrating the presence of 7 macrophages (3D surface - red) close to PLA-NP (cyan) within the caudal vein plexus area. Both opening of the stack with a clipping plane (D') and the optic sections (D") reveal internalizations of PLA-NP by macrophage from the lumen (white arrowheads – 1, 5, 6) and outside the lumen (yellow arrowhead - 7). (B-B′) 17 μm MIP (x60 objective) from which (B″) is a 1 μm thick optical section. (C) 50 μm MIP (x60 objective). (D) 13 μm MIP (x60 objective) with a 3D surface reconstruction of the macrophage fluorescence signal. (D') illustrates an opening the MIP with a clipping plane, while (D") is a 1 μm thick optic section from the stack. Annotations: B, brain; CA, caudal artery; CVp, caudal vein plexus; DA, dorsal aorta; DLAV, dorsal longitudinal anastomotic vessel; E, eye; H, heart; IsV, intersegmental vessel; Lu, lumen; PCV, post-cardinal vein; SiV, sub-intestinal veins; Y, yolk. Scale bars: 200 μm (A), 100 μm (A'-A"), 20 μm (C) and 10 μm (B-B″, D-D"). (For interpretation of the references to colour in this figure legend, the reader is referred to the web version of this article.)

longitudinal anastomotic vessels and the sub-intestinal vein are shown in (Fig. S2) and into the cerebral blood vessels and liver sinusoids (Fig. S3). We also localized PLA-NP inside endothelial cells forming the endocardium of the atrium and the ventricle of the heart (not shown).

2.3. Internalization of PLA-NP by professional phagocytes

In order to identify the cells that were accumulating PLA-NP inside the bloodstream at the caudal vein plexus, we focused on the phagocytes already present in the zebrafish embryo at 3 days post-fertilization: macrophages and neutrophils. Therefore, we first injected green fluorescent PLA-NP (5 mg/mL) into mpeg1:mCherry transgenic zebrafish [23], whose macrophages express a red fluorescent cytosolic protein. Two hours later, 3D live-imaging acquisitions at the caudal vein plexus, a region where macrophages are abundant, clearly showed the internalization of PLA-NP by macrophages residing within the lumen (macrophages #1–2–3-5-6) and outside the blood vessel (#7). In addition, macrophages devoid of PLA-NP could also be observed (#4) (Figure: D-D"). A 3D reconstruction of the acquired image is presented in (Video S2). By contrast, neutrophils, labelled in mpx:GFP zebrafish [24], showed no detectable interaction with red fluorescent PLA-NP, even when the particles were injected at higher concentration (10 mg/mL) (Video S3).

2.4. Dynamic of PLA-NP biodistribution from 30 min to 24 h by light microscopy

The biodistribution of NP at a given time is crucial information to understand how the particles interact with the organism and allow one to better design the therapeutic strategy. The above observations showed that PLA-NP could enter endothelial cells and macrophages in significant amounts. We next investigated the kinetics of this uptake process by regular observations (30 min, 4 h and 24 h) following injection of fluorescent PLA-NP in 3 dpf zebrafish (either fli:GFP or mpeg1:mCherry). We then focused on the co-localization of PLA-NP with respect to selectively labelled endothelial cells and macrophages.

Although we monitored live embryos, here we favored the use of cryosections over live-imaging to analyze samples at precise time points and visualize the internal organs in more detail. The cryosections were prepared with a thickness of 30 μm and imaged in the center to avoid the risk of the artefactual displacement of NP, which from our experience is inherent to thinner cryosections (< 20 μm) [15].

The high-resolution imaging of the cryosections confirmed that, once in the circulatory system, fluorescent PLA-NP were promptly taken up by endothelial cells. After 30 min following the administration (Fig. 2: A-A'), while no fluorescence from PLA-NP could be detected inside the bloodstream, strong accumulations of PLA-NP were present inside endothelial cells. These accumulations showed a scattered distribution inside the endothelial cells. At later time-points, 4 h and 24 h post-injection, the association of PLA-NP with endothelial cells was still observed, increasingly, the accumulation of NPs formed massive clusters adjacent to the nucleus (Fig. 2: B-C′), presumably in endocytic organelles [25].

Like the endothelial cells, macrophages were quick to internalize fluorescent PLA-NP, as seen 30 min following the intravenous injections (Fig. 2: D). No striking changes in the localization pattern inside macrophages could be detected at later time-points (Fig. 2: *E*-F). Intriguingly, although based on qualitative observations, we noticed that the fluorescence signal from the PLA-NP seemed more intense in some macrophages at the 24 h time-point. In addition, during our observation on fli:GFP fish, we could observe phagocytes with high concentrations of PLA-NP outside the bloodstream at the 24 h time-point (Fig. 2: C, C′, star).

Finally, by investigating the whole fish, we could evaluate the capacity of PLA-NP to reach certain internal organs: the brain, the kidney and the liver. In the brain, aside from the internalization of PLA-NP by the endothelial cells that form the cerebral blood vessels, no leakage to the parenchyma could be observed at any time-point (Fig. S3: A-C). At this stage, the blood-brain barrier is functional [26]. We could however observe bright accumulations of PLA-NP in a few cells outside the vascular compartment at 24 h post-injection. These cells were later identified as brain macrophages, *e.g.* microglia (Fig. S3: D). The kidney, where glomerular filtration is operational in 3 dpf zebrafish [27], is responsible of the excretion of small material (< 8 nm of hydrodynamic diameter) [28], We could not detect any sign of fluorescence associated to PLA-NP inside the pronephric ducts of the kidney at any time-points. In contrast to mammals, the liver of teleosts plays little role in the reticulo-endothelial system [29]. Still, PLA-NP were internalized by endothelial cells from the sinusoidal vessel, as well as by rare hepatocytes at latest time-point (Fig. S3: *E*-G).

2.5. Dynamic of PLA-NP biodistribution from 10 min to 7 days by electron microscopy

One of the limitations of light microscopy is that its resolution usually does not allow the direct observation of individual NP of 200 nm or below. Therefore, we complemented our observations from light microscopy with the use of transmission electron microscopy to study the biodistribution of PLA-NP at the sub-cellular level. There, we widened the time-span of the experiments (from 10 min to 7 days) to both witness the internalization of PLA-NP and evaluate their integrity over time. Because the poly(lactic-acid) polymer is non-dense to the electrons, in order to facilitate the identification of PLA-NP on electron micrographs, 6–7 nm electron-dense hydrophobic colloidal gold particles were

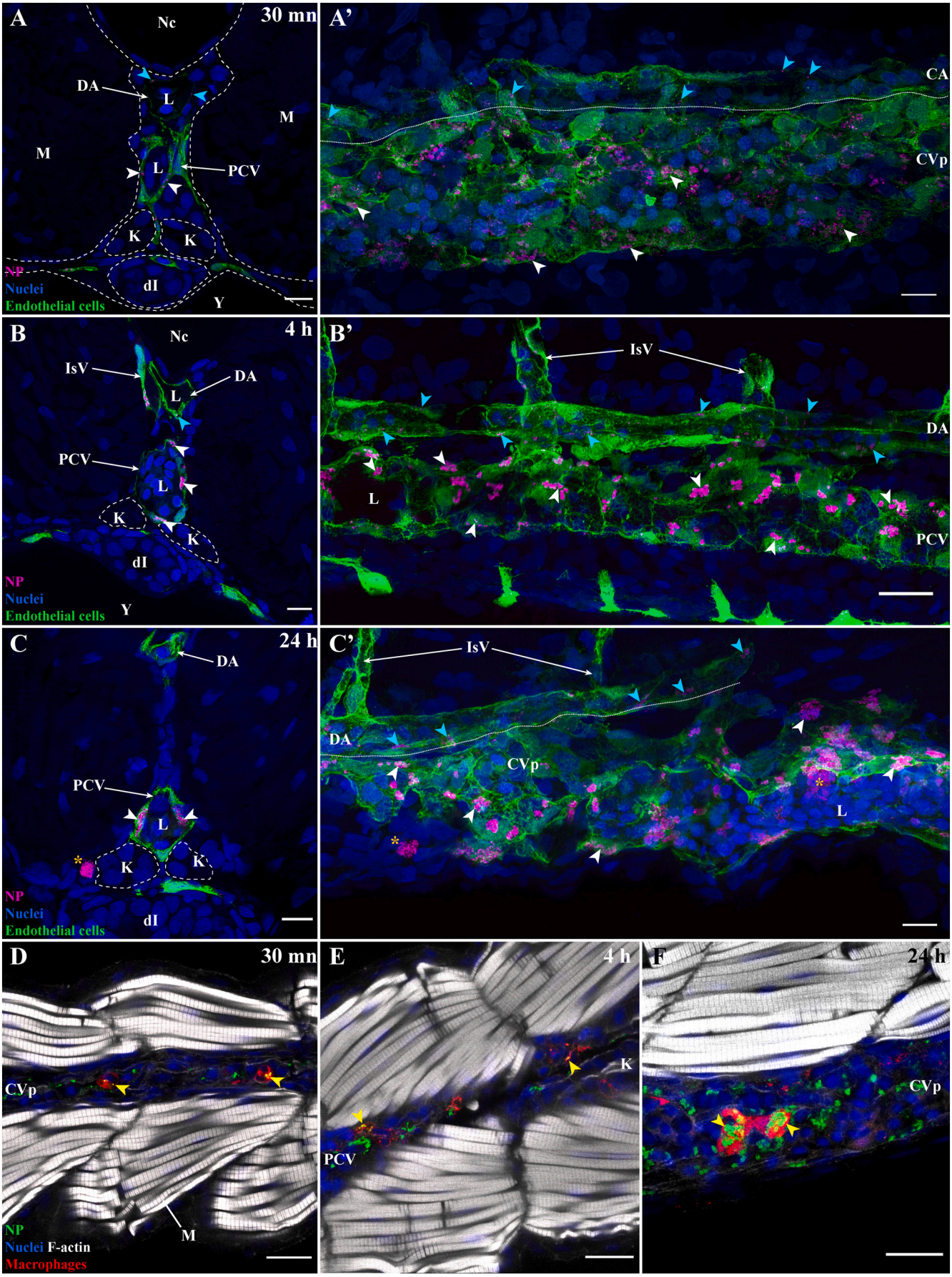

(caption on next page)

Fig. 2. Dynamics of PLA-NP internalization by endothelial cells and macrophages at 30 min, 4 h and 24 h post-injection. Representative images of 3 dpf fli:GFP zebrafish transversally sectioned (A, B, C), para-sagitally sectioned (A',B′,C′) and of 3 dpf mpeg1:mCherry zebrafish para-coronally sectioned (D-F). Images were acquired from 30 μm thick whole-organism cryosections. Images (A-C′) highlight PLA-NP (magenta), endothelial cells (green) and nuclei (blue), while images (D-F) highlight PLA-NP (green), macrophages (red), F-actin (white) and nuclei (blue). (A,A') The internalization of NP by endothelial cells from both veins (white arrowheads) and artery (cyan arrowheads) was already evident 30 min post-administration while no free-circulating PLA-NP could be observed within the blood flow. From this timepoint, no further change in the distribution of PLA-NP among endothelial cells from vein (white arrowheads) and artery (cyan arrowheads) could be detected 4 h (B-B′) and 24 h (C-C′) later, apart from the aggregation of the PLA-NP overtime (A',B′,C′). Note the presence of large aggregates of PLA-NP within phagocytes outside the lumen at the 24 h timepoint (C-C′ – orange stars). Similar observations apply to the internalization of PLA-NP by macrophages with uptake (yellow arrowheads) observed 30 min (D), 4 h (E) and 24 h (F) post-administration. While only qualitative, observations of PLA-NP accumulation among macrophages suggested they were larger at 24 h (F) than at 30 min (D) post-administration. (A,B,C) 1 μm MIP (x60 objective). (A') 20 μm MIP (x60 objective). (B′) 13 μm MIP (x60 objective). (C′) 22 μm MIP (x60 objective). (D,E,F) single optical sections (x60 objectives). Annotations: CA, caudal artery; CVp, caudal vein plexus, DA, dorsal aorta; dI, developing intestines; K, kidney; L, IsV, intersegmental vessel, lumen; M, muscles, Nc, notochord; PCV, post-cardinal vein; Y, yolk. Scale bars: 20 μm (A',B′,*E*-F) and 10 μm (A,B,C-D). (For interpretation of the references to colour in this figure legend, the reader is referred to the web version of this article.)

encapsulated into the PLA-NP. PLA-NP(gold) then appeared as pale spheroids with internal electron dense particles under the electron-beam (Fig. S4).

Within 10 min after the injection, single non-aggregated PLA-NP were still circulating inside the bloodstream while others were already internalized by endothelial cells (Fig. 3: A). We could witness all the steps of PLA-NP internalization from their association to the plasma membrane to their accumulation into the intracellular *endo*-membrane system. While the precise internalization pathways in the cells remain to be characterized, some associations of individual PLA-NP with coated invaginations of the plasma membrane of endothelial cells were highly suggestive of a clathrin-mediated internalization (Fig. 3: B). In addition, figures resembling phagocytosis were also observed (Fig. 3: C). Once internalized, the PLA-NP loaded cellular compartment appeared to fuse into larger cellular structure containing numerous particles (Fig. 3: D). In contrast to the highly dynamic behavior of PLA-NP observed 10 min following the injection, 20 min later PLA-NP were heavily concentrated inside cellular compartments of endothelial cells while none remained inside the blood vessel (Fig. 3: E). The biodistribution of PLA-NP remained largely unchanged at the 4 h and 24 h time-points (Fig. 3: F-G). These results confirm and extend the observations we made from light microscopy, and reveal that the bright fluorescence clusters we observed represent in fact a strong accretion of PLA-NP that occurred after internalization in cells.

Whether internalized by endothelial cells or by phagocytes, the integrity and the colloidal stability of PLA-NP endured the first 24 h post-injection (Fig. 3: F-G). It was only after 3 days following the injection that change in the morphology of PLA-NP could be seen. Among some endothelial cells, gold particles were seen apparently being released from the matrix of PLA-NP; a possible consequence of an early PLA-NP degradation (Fig. 3: H). This change was more pronounced 24 h later (4 days post-injection). While PLA-NP remained intact in some endothelial cells (Fig. 3: I), in others, a shrinkage of PLA-NP was observed, in addition to the release of gold particles (Fig. 3: J). One week after injection, the heterogeneity of PLA-NP disassembly inside endothelial cells was striking. In some endothelial cells, the structure of the PLA-NP was entirely lost, only a paste of amorphous PLA mixed with gold particles remained (Fig. 3: K-L). In other cells, shrunken PLA-NP persisted along with released gold particles (Fig. 3: M). Finally, in some endothelial cells only aggregates of free gold particles remained visible (Fig. 3: N). These results indicate that an augmented release of an encapsulated cargo from surfactant-free PLA-NP could start around one week after intravenous administration.

2.6. Complementary information regarding the internalization of PLA-NP by endothelial cells

To deepen our understanding of the internalization of PLA-NP by endothelial cells, we complemented our investigations with additional live-imaging experiments.

Our previous data indicated that PLA-NP clearance occurs in the first 30 min following the administration. Videos of these first 30 min following the injection revealed that most of the fluorescent PLA-NP had already been taken-up by endothelial cells from both veins and arteries in the few minutes required to prepare the samples before the acquisitions (anesthesia-mounting-setting acquisition parameters) (Fig. S5: A-D'). As illustrated with Video S4, the clearance of PLA-NP from the blood seems to occur in around 20–25 min. Indeed, few PLA-NP could be detected inside the lumen of blood vessels at the beginning of the videos while this amount decreased overtime and past the 20th minute, almost none could be observed in the blood flow (Fig. S5: E-J).

We then investigated if the internalization of our anionic PLA-NP by non-scavenger endothelial cells [19] could be dependent of the amount of administered PLA-NP. In most of our previous experiments, PLA-NP were injected at a concentration of 5 mg/mL. Here we analyzed the biodistribution (30 min) of PLA-NP injected at different concentrations, ranging from 1 mg/mL to 10 mg/mL (Fig. S6-8), For all the different concentrations, the revealed biodistribution was similar to the one we previously described, suggesting that PLA-NP internalization by non-scavenger cells is not dependent on the saturation of the scavenger endothelial cells.

Campbell et al. [19] showed that internalization of numerous anionic NP, which are restricted to the scavenger endothelial cells, is charge-dependent and could be inhibited with a pre-treatment of intravenously injected sulfate dextran (40 KDa) to saturate the scavenger receptor stab2. We then decided to verify if the internalization of our PLA-NP by scavenger and non-scavenger endothelial cells followed similar rules. As dextran sulfate 40 KDa is quite toxic for fish, we applied the refined protocol published by Verweij et al. [30] which instead use a pre-treatment of dextran sulfate (500 KDa) for reduced adverse effects. This pre-treatment, with 3 mg/mL of sulfate-dextran 500 KDa 2 h before the PLA-NP injection, strongly reduced the internalization of PLA-NP by the scavenger endothelial cells while the internalization by non-scavenger endothelial seemed unaffected (Fig. S7: A-B′, D-E). In this configuration, the presence of PLA-NP in the blood flow 30 min following their injection was striking. This experiment suggests that while the internalization of PLA-NP by the scavenger endothelial cells seemed to follow the rules described by Campbell et al. [19], the internalization of PLA-NP by non-scavenger endothelial cells seemed to involve other mechanisms that are independent of the negative-charge of the particles. To evaluate if these other mechanisms could clear the PLA-NP from the blood, we applied a stronger sulfate-dextran pre-treatment (30 mg/mL) and analyzed the biodistribution of PLA-NP 3 h after the injection. We obtained similar results, indicating that the charge-dependent internalization by scavenger endothelial cells appears to be the main driving force behind the clearance of PLA-NP from the blood (Fig. S7: C-C′). Noteworthy is that significant internalization of PLA-NP by phagocytes could still be observed (Fig. S7: F).

2.7. Continuous internalization of PLA-NP by macrophages during the first 24 h

Throughout our investigations, we came across several intriguing peculiarities regarding the internalization of PLA-NP by macrophages.

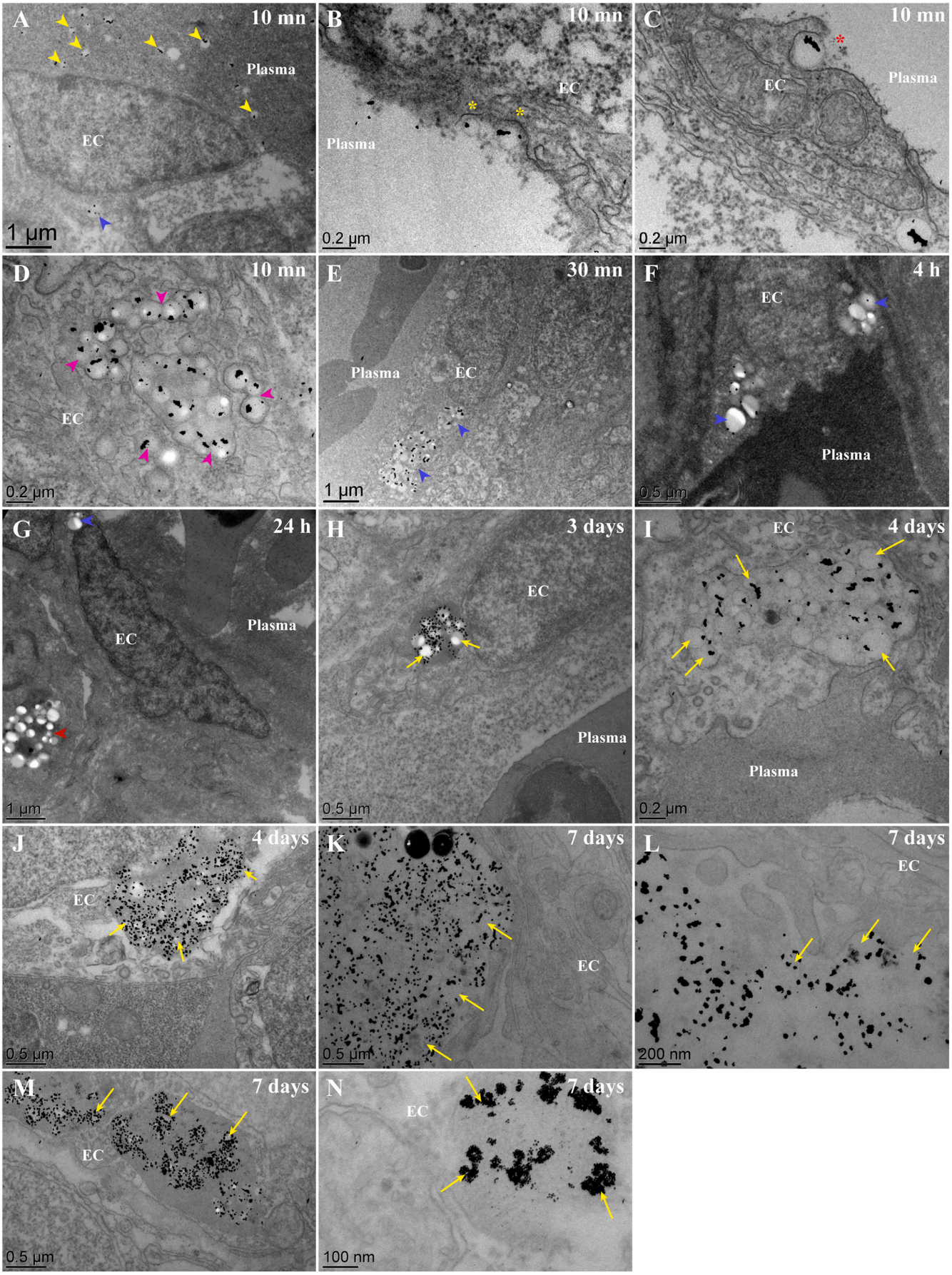

(caption on next page)

Fig. 3. Fate of PLA-NP(Gold) once internalized by endothelial cells, from 10 min to 7 days post-injection, as observed with TEM. Representatives electron micrograph of ultrathin (60 nm) epon sections from zebrafish larvae injected at 3 dpf with PLA-NP encapsulating gold particles (<10 nm), 10 min (A-D), 30 min (E), 4 h (F), 24 h (G), 3 days (H), 4 days (I-J) and 7 days (K-N) post-injection. (A-D) 10 min following intravenous injection, PLA-NP are circulating within the bloodstream (A - yellow arrowhead) and internalized by endothelial cells (A - blue arrowhead). Internalization of PLA-NP by endothelial cells involve an invagination of the plasma membrane, resembling clathrin-mediated internalization (B - yellow stars), as well as figures resembling phagocytosis (C – red stars). Numerous NP were already being condensed within cellular compartment of some endothelial cells (D – magenta arrowheads). 30 min after the injection, no more PLA-NP could be observed within the bloodstream, in contrast to the massive concentration of PLA-NP within endothelial cells (E - blue arrowhead). No sign of degradation could be observed from PLA-NP internalized by endothelial cells (A, *E*-G - blue arrowhead) and underlying phagocytes (G - red arrowhead) during the first 24 h. Starting from 3 days post-injection, change in the colloidal stability of internalized PLA-NP was evident in some cells, encapsulated gold-particles being released from the NP-PLA matrix (H - yellow arrows). PLA-NP degradation was seemingly more pronounced 4 days post-injection, within some endothelial cells PLA-NP could are observed with a shrunken size (I - yellow arrows) while in others there are more gold crystals free rather than inside the PLA matrix (J - yellow arrows). Finally, a week after the injection different shade of PLA-NP degradation could be observed inside endothelial cells, cellular compartment filled with a paste of amorphous PLA containing gold crystals (K-L - yellow arrows), shrunken PLA-NP with released gold crystals (M - yellow arrows) and cellular compartment where only aggregated gold crystals remain (N - yellow arrows). Annotations: EC, endothelial cell. Scale bars: 1 μm (A,E,G), 500 nm (F,H,J-K,M), 200 nm (B-D,I,L) and 100 nm (N). (For interpretation of the references to colour in this figure legend, the reader is referred to the web version of this article.)

For example, it seemed that macrophages could display a more intense PLA-NP fluorescence signal at 24 h than at 30 min post-injection (Fig. 2: *E*-F). In addition, the accumulation of PLA-NP by brain macrophages also raised the question of how could these cells access PLA-NP (Fig. S3: A-D)? Altogether, these elements suggested that the internalization of PLA-NP by macrophages might not be restricted to the first 30 min. We therefore decided to quantify the dynamic of PLA-NP internalization by macrophages in more detail. Because of the minuscule size of the NP, we combined live imaging and flow cytometry to obtain reliable quantification of the PLA-NP uptake by macrophages.

We first performed an automated analysis of the quantity of PLA-NP fluorescence that associate with macrophages using stereomicroscope live-acquisitions and an ImageJ macro previously developed [31]. In agreement with the observations from light microscopy, the automated analysis revealed an increase (plus 56%) in the amount of PLA-NP inside macrophages between 30 min and 24 h (Fig. 4: A). We then performed a flow-cytometry experiment on mpeg1:mCherry zebrafish injected with green fluorescent PLA-NP (2,5 mg/mL) to quantify the fraction of macrophage (mCherry+ cells) involved in the uptake of PLA-NP (Fig. 4: B-B′). Already 10 min after the injection, 8% of the macrophages already contained detectable PLA-NP. The fraction of PLA-NP- containing macrophages then steadily increased until it plateaued around 17% between 4 and 24 h. It is important to note that at this stage, numerous new macrophages are continuously being generated, increasing the pool of PLA-NP negative macrophages over the course of the experiment. Not only could we confirm the continuous uptake of PLA-NP by macrophage, these results also raised an important question: how do macrophages continue to internalize PLA-NP when none remains in the bloodstream, most of them being internalized by endothelial cells?

2.8. Evidence for a transfer of PLA-NP from endothelial cells to macrophages

We thus hypothesized that macrophages might take up PLA-NP from endothelial cells, and focused our efforts on 3D live-imaging after the 30 min timepoint to witness such events. With only a few cells separating it from the exterior environment, the flat endothelial layer surrounding the yolk (Yolk circulation valley) is a favorable region to perform dynamic 3D live-imaging at a high-resolution (Fig. S1). In this region, as illustrated (Fig. S10: A), macrophages are also abundant. During our preliminary image acquisitions, we could assess the internalization of green fluorescent PLA-NP by red fluorescent macrophages, as illustrated (Fig. S10: B-F, Video S5) by a video made 70 min post-injection. At start, this video display a PLA-NP negative macrophage moving to the close proximity of a cell with PLA-NP within cellular compartments, likely an endothelial cell. Following several minutes of apparent contact, the macrophage moved away, then displaying PLA-NP-loaded cellular compartments. This initial investigation suggested the intriguing possibility of a peculiar cell-to-cell transfer of PLA-NP.

We deepened our investigations with the injection of far-red fluorescent PLA-NP in double transgenic zebrafish fli:GFP and mpeg1:mCherry to reveal any potential transfer of material between endothelial cells and macrophages. Both PLA-NP+ endothelial cells and PLA-NP+ macrophages were present in the area, 30 min post-injection (Fig. 5: A). There, we could witness striking transfers of GFP-labelled fragments of endothelial cell cytoplasm, containing far-red fluorescent PLA-NP, from endothelial cells to macrophages. An illustration of the transfer is presented (Fig. 5: B-I, Video S6) with a 3D video acquired 30 min post-injection. In this video, a PLA-NP containing macrophage in the bloodstream can be seen moving very close to PLA-NP-positive endothelial cells. Then, less than 10 min later, internalization of a surprisingly large amount of GFP+ material could be observed inside the macrophage. The optical sections isolated from the video reveal the presence of PLA-NP among the GFP+ internalized material (Fig. 5: J-K). On a 3D image acquisition made after the video, the same macrophage could be seen with a mix of small PLA-NP+ / GFP- cellular compartments, a large PLA-NP+ / GFP+ cellular compartment and a bright GFP+ spot on its plasma membrane (Fig. 5: L-L"). Interestingly, the GFP fluorescence signal seemed more faint (compare Fig. 5: J and Fig. 5: L), possibly because of the acidity of the presumed late endocytic organelle where the NP resided that might be quenching the GFP signal [25].

It is important to note that during the transfer of NP, no GFP fluorescence signal could be observed inside the cytosol of macrophages, likely ruling out the formation of direct openings connecting the cytoplasm of both cells. No cell death could be observed among the donor cells and the neighboring endothelial cells. In addition, using acridine orange to further analyze cell death (Fig. 5: M) [32,33], we found that the intravenous injection of PLA-NP only induced the same level of cell death as the mock-injection after 30 min, likely caused by the mechanical injury. The fish then fully recovered 24 h after the injection, with all cell death level returning the level measure from non-injected fish. Overall, our observations indicate that NP transfer from endothelium to macrophage involve cell-to-cell handover of large cytoplasmic bundles, the precise mechanisms of which remain to be elucidated.

2.9. Evidence of a microvesicle-like transfer from endothelial cells to macrophages

During our investigation, we also encountered the transfer of microvesicle-like structures from endothelial cells to macrophage. This phenomenon is illustrated in (Fig. 6, Video S7). The video first shows the formation of a GFP-labelled microvesicle-like structure budding out of an endothelial cell from the caudal vein plexus (Fig. 6: A-B). After a few minutes, the microvesicle-like structure was then released from the endothelial cell (Fig. 6: C) into the lumen of the blood vessel. The microvesicle-like structure was then quickly internalized by an adjacent macrophage in the bloodstream (Fig. 6: D). Interestingly, the fluorescence signal of the GFP-labelled microvesicle-like structure started to fade after being taken up by the macrophage, until it was no more detectable 13 min later (Fig. 6: *E*-H).

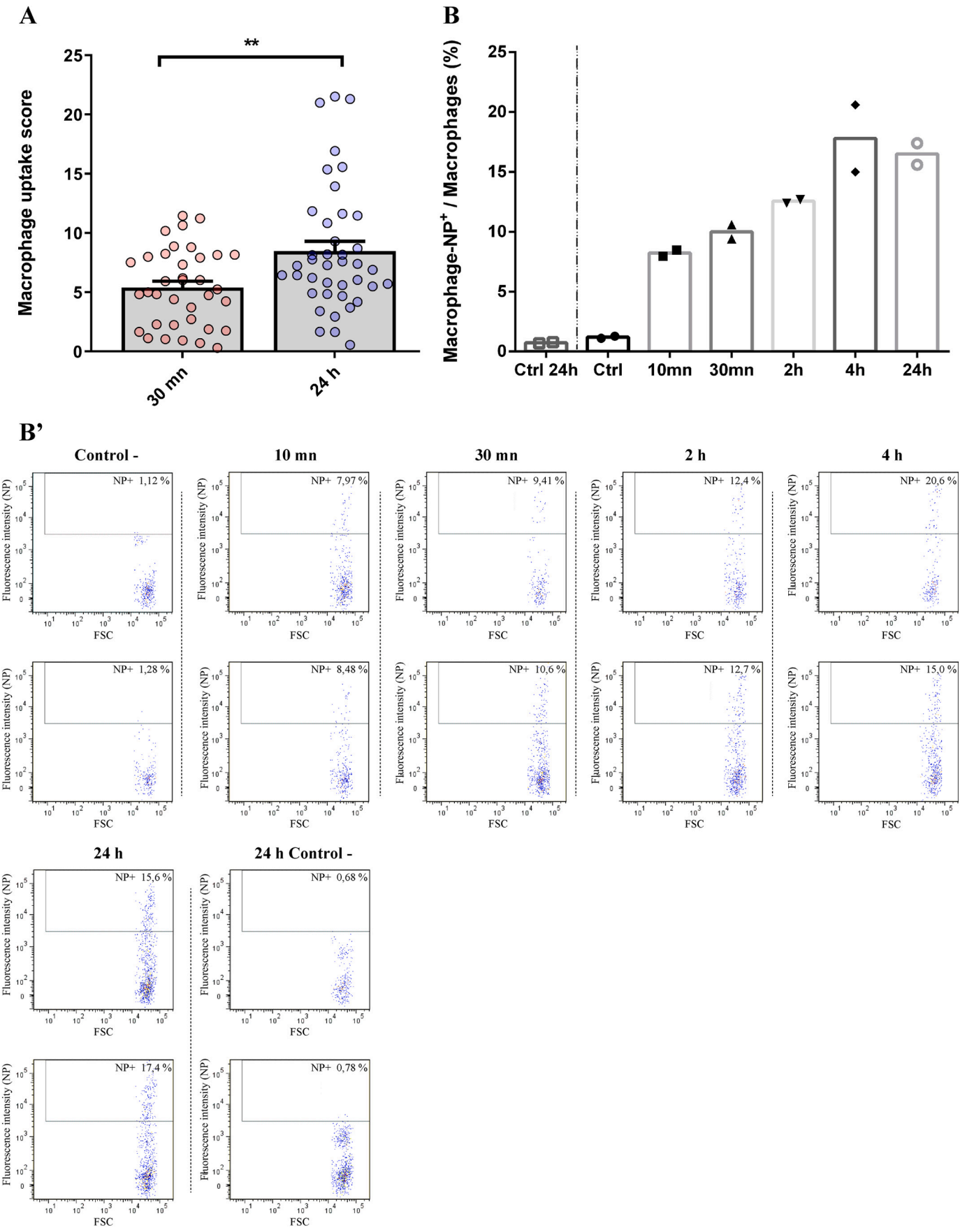

(caption on next page)

Fig. 4. Quantitative analysis of PLA-NP internalization by macrophage from 10 min to 24 h post-injection. (A) Automated analysis of the relative amount of internalized fluorescent PLA-NP by macrophage 10 min and 24 h following intravenous injection of 3 dpf mpeg1:mCherry zebrafish. Stereo-microscope acquisitions of individual zebrafish were put through an ImageJ macro, from which an internalization score was calculated, based on the amount of red PLA-NP fluorescence associating with the green macrophage fluorescence signal, relative to the total amount of red PLA-NP fluorescence detected from the whole fish. Histograms represent the mean internalization score and each dot represents the score of an individual zebrafish. From 30 min to 24 h post-injection, more NP were internalized by macrophages (+56%). (B) Flow cytometry analysis of the fraction of macrophages that had internalized fluorescent PLA-NP relative to the whole population of macrophages, 10 min to 24 h after intravenous injection into 3 dpf zebrafish. Histograms represent the mean percentage of PLA-NP positive macrophages at different time-points following administration, with each dot representing the data acquired from 10 pooled larvae. Almost 8% of macrophages were labelled positive for PLA-NP 10 min after the injection. After this time, the fraction of macrophage internalizing PLA-NP steadily increased over time until it reached a plateau around 17% of PLA-NP-positive macrophages at 4 h and 24 h post-injection. All the flow-cytometry acquisitions are illustrated in (B′), they only display the population of macrophage which was gated based on the mCherry fluorescence intensity. The x axis displays the "size" of the detected events and the y axis the fluorescence intensity corresponding to PLA-NP. Error bars: SEM. Significance level is indicated as: $^{**}p < .01$. Number of fish per condition: (A) 30 min (36) and 24 h (40); (B) 10 larvae per replicate. (For interpretation of the references to colour in this figure legend, the reader is referred to the web version of this article.)

The isolated optical sections from the video highlight the attachment of a GFP-labelled microvesicle-like structure to the macrophage plasma membrane (Fig. 6: I), followed by its internalization inside a mCherry negative cellular compartment (Fig. 6: J). We could not detect any PLA-NP inside the microvesicle-like structures during our observations. However, our data still do not allow us to rule out the possibility of a PLA-NP transfer by such a mechanism. Indeed, as illustrated (Fig. 6: K-L") in a 3D acquisition, we could observe the presence of PLA-NP, inside endothelial cells, that were in very close proximity to budding endothelial microvesicle-like structures. This budding microvesicle-like structures are also embraced by macrophages, that here co-internalized PLA-NP+ and GFP+ labelled materials.

3. Discussion

The objective of the present study was to evaluate the biodistribution of intravenously injected surfactant-free PLA-NP *in vivo* and with a high resolution using the zebrafish model. The goal behind the design of our surfactant-free PLA-NP was to follow the 'safe-by-design' paradigm of developing the most compatible NP for human applications [9,10]. Almost nothing is known about surfactant-free NP *in vivo*, hence our aim was to initiate the analysis of surfactant-free PLA-NP *in vivo* and not to make a direct comparison between PLA-NP with, or devoid of surfactant. Using a combination of live-imaging, cryosections and electron microscopy (EM), our study reveals rapid internalization of NP throughout the vascular endothelium of the zebrafish embryo, as well as into macrophages. We introduce a method allowing colloidal gold particle to be encapsulated in PLA-NP, opening the door for visualizing these NP at the ultrastructural level. Finally, by using automated imaging analysis, flow-cytometry and live-imaging we describe a striking transfer of NP from endothelial cells to macrophages.

In recent years the zebrafish has emerged as a powerful animal model for the study of nanomedicine *in vivo*, especially for live-imaging at a high resolution, as discussed in depth by Sieger et al. [34] It has, for example, recently been used for the live-imaging study of endogenous particles in the nanosized range such as exosomes [35] and tumor extracellular vesicles [36]. In our study, the negatively-charged PLA-NP were quickly internalized by macrophages and by both venous and arterial endothelial cells distributed along the entire vasculature (Fig. 1-2). The internalization of PLA-NP by endothelial cells was stronger in veins than arteries. Once internalized by endothelial cells, PLA-NP did not reach the cytosol and remained in vesicles from the endomembrane system, an aspect of their biodistribution we later confirmed using electron microscopy (Figs. 1–3).

The internalization of our PLA-NP into endothelial cells from all the blood vessels, veins and arteries, was surprising for an anionic NP. Others have described the uptake of different NP by endothelial cells. In a recent study, Campbell *et al* [19] demonstrated that the internalization of a wide range of negatively charged NP (liposomes, polymersomes, polystyrene NP, virus-like particles) was restricted to specific venous regions of zebrafish embryos, namely: the caudal vein plexus, the dorsal aspect of the post-cardinal vein and the primary head sinus. In these blood vessels, the highly endocytic scavenger endothelial cells resemble the mammalian sinusoidal endothelial cells. This pattern of biodistribution, where no NP are internalized by endothelial cells from arteries, has been observed in multiple studies using different families of negatively charged NP [20,21,37]. Even the recent studies on nano-sized endogenous exosomes and tumor extracellular vesicles also described this selective uptake by the scavenger endothelial cells forming the caudal vein plexus [35,36]. Hence, besides showing that our PLA NP can also be internalized by endothelial cells, our study also reveals a pattern of endothelial cell uptakes that was unprecedented for negatively-charged NP. Intriguingly, in the Campbell study [19] it was the positively charged liposomes that displayed a biodistribution similar to our PLA-NP. Our results then further highlight the difficulty of predicting NP biodistribution and raise an important question: why would our anionic PLA-NP behave like cationic NP and not like the other negatively charged NP? Interestingly, our complimentary experiment provided some insight to this question (Fig. S5-S9). The main mechanism responsible of the clearance of PLA-NP is a negative-charge-dependent internalization by the scavenger endothelial cells, in agreement with the model proposed by Campbell et al. [19]. However, they also revealed the involvement of one or several additional mechanism(s) that work in a negative-charge independent manner and that are responsible of the internalization of PLA-NP by the non-scavenger endothelial cells, either venous or arterial. In addition, these unidentified mechanism(s) do not result from a saturation of charge-dependent-mechanism involving the scavenger endothelial cells but occurs at the same time. Still, why only our PLA-NP are internalized this way and not the other described anionic NP remains a mystery.

Using thin cryosections to evaluate the capacity of PLA-NP to escape the vasculature, our results indicate that relatively few PLA-NP accumulate inside internal organs (Brain, Kidney, Liver, *etc.*) (Fig. 2, Fig. S3). This intrinsic targeting of endothelial cells from the whole vasculature by PLA-NP, with minimum accumulation inside internal organs, could be an interesting finding for developing strategies for the treatment of vascular-related diseases.

An important aspect of our study was to evaluate the fate of PLA-NP by both light microscopy and electron microscopy (Figs. 2-3). Although EM can visualize NP in detail it is rarely used to study the fate of nano-sized particles *in vivo* [13,22,35,36]. One of the challenges of using EM to study NP *in vivo* is the preservation and visualization of their structure in order to unequivocally identify them in electron micrographs. A novel approach we developed allowed encapsulation of electron-dense gold particles in the matrix of PLA-NP to guarantee their identification in electron micrographs. This enabled us to observe internalization of our PLA-NP by endothelial cells by clathrin-mediated endocytosis and a process resembling phagocytosis, as soon as 10 min post injection. The high activity of endothelial cells toward PLA-NP is consistent with these cells being highly active in clathrin-mediated endocytosis [38,39] and being able to phagocyte bacteria [40].

Subsequent to their internalization by endothelial cells, PLA-NP were concentrated within vesicles, likely from the endocytic system [25]. Our study reveals that while the distribution of PLA-NP remained almost

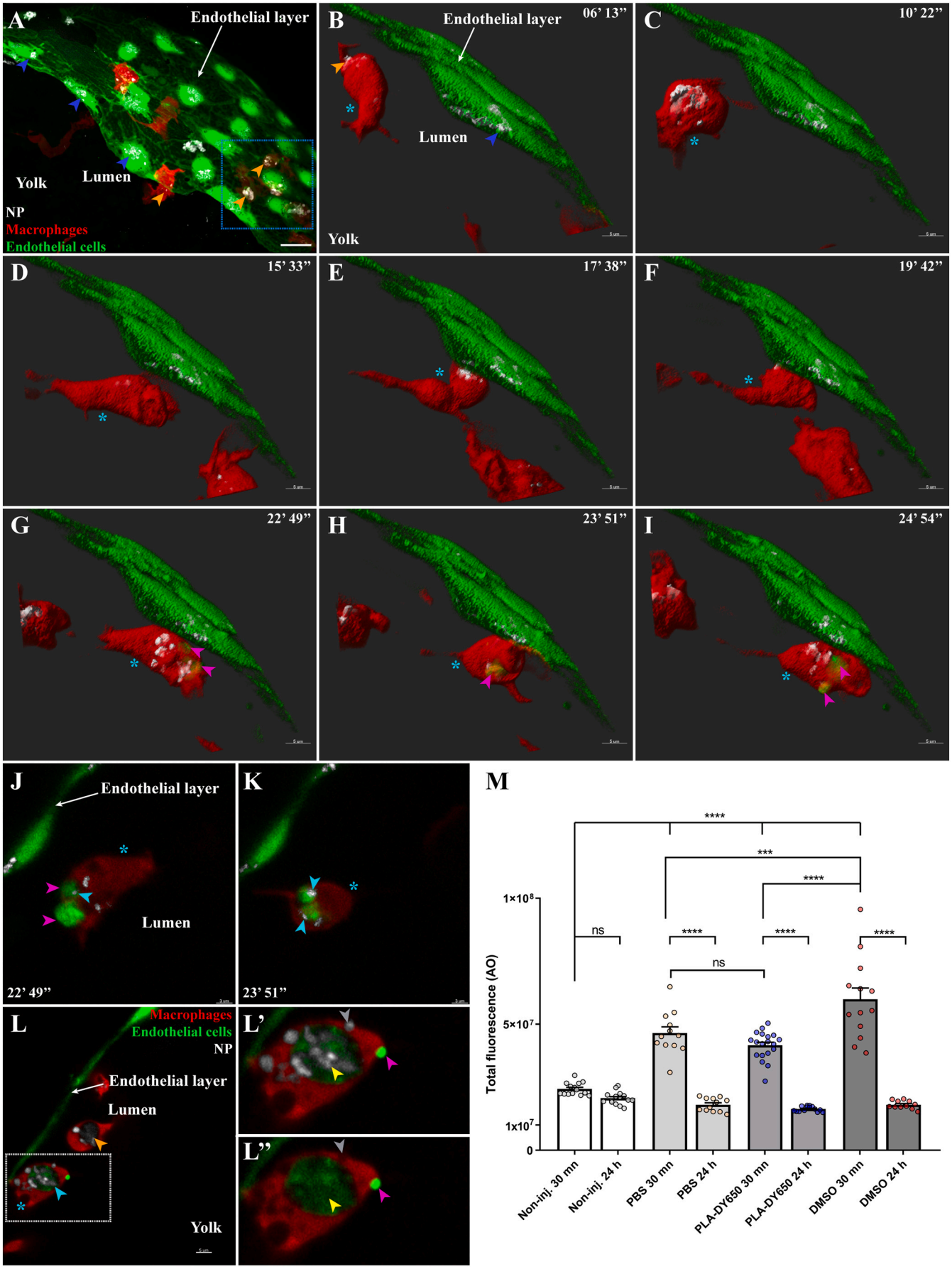

(caption on next page)

Fig. 5. Transfer of PLA-NP from endothelial cells to macrophages. Representative live-acquisitions of 3 dpf mpeg1:mCherry and fli:GFP double transgenic zebrafish, 30 min after the intravenous injection of far-red fluorescent PLA-NP and using a spinning-disk confocal microscope. The acquisitions were made at the yolk circulation valley as illustrated in (A – 53 μm MIP, x63 objective), endothelial cells and macrophages being represented as a 3D surface reconstruction (green and red, respectively) and where PLA-NP (white) internalized by endothelial cells (blue arrowheads) and macrophage (orange arrowheads) can be observed. (B-I) The video (14 μm MIP), made across PLA-NP+ endothelial cells (blue arrowhead) of the endothelial layer covering the yolk, focuses on a macrophage (cyan star) which is already PLA-NP+ (orange arrowheads). At first, the macrophage enters in the proximity of the PLA-NP-positive endothelial cells (B-D). After almost 10 min at this position (*E*-F), GFP-labelled fragments of endothelial cell can be observed within the macrophage (G-I - magenta arrowheads) while the endothelial cells remain alive (J-K). Optical sections (1 μm) from G and H respectively, indicate the presence of PLA-NP (cyan arrowheads) inside the GFP-labelled fragment of endothelial cells (magenta arrowheads) that have been transferred to the macrophage (cyan star). (L) On an acquisition few minutes after the video, PLA-NP can be seen inside a GFP-negative macrophage (orange arrowhead), and within the GFP+ macrophage (cyan star and arrowhead). (L'-L") A close-up of the latter macrophage shows the presence of GFP-/PLA-NP+ cellular compartment (grey arrowhead), along with a massive GFP+/PLA-NP+ one in which both PLA-NP and the GFP+ cytosolic fragments of the endothelial cell co-localize (yellow arrowhead). Note the presence of a bright GFP+ structure at the surface of the macrophage (magenta arrowhead). (M) Analysis of the cell death following PLA-NP injection, assessed by the overall acridine orange fluorescence intensity (y-axis) of the whole zebrafish by stereomicroscopy. Intravenous injection of PLA-NP (DY650) does not induce cell death other than the mechanical injury from the injection, which is healed by 24 h post-injection. Each dot represents one single individual. Error bars: SEM. Significance level is indicated as: ***$p < .001$ and ****$p < 0{,}0001$. Number of fish per condition (30 min / 24 h): Non-injected (14 / 15), PBS-injected (12 / 12), PLA-DY650-injected (19 / 14), DMSO-injected (13 / 11). Scale bars: 20 μm (A), 5 μm (B-I,L) and 3 μm (J-K). (For interpretation of the references to colour in this figure legend, the reader is referred to the web version of this article.)

unchanged during the first 24 h post-injection, they started to progressively lose their colloidal stability 72 h after being taken up by endothelial cells. The complete disassembly and release of gold particles from within some PLA-NP became evident after 1 week. Very few studies have been able to analyzed the disassembly of NP *in vivo* using imaging techniques [37].

Macrophages and neutrophils are immune cells that are involved in the clearance of foreign materials. Devoid of stealth properties, such as the one conferred by polyethylene (PEG) [41] or polysarcosine [42,43], our PLA-NP remained relatively briefly in the circulation and were rapidly engulfed by macrophages, as we expected. Many NP lacking stealth properties, such as PLGA [14], liposomes [19,44] and polymersomes [45], have been shown to be rapidly taken up by macrophages when intravenously injected into zebrafish larvae, a phenomenon that is also seen in higher vertebrate models [44]. However, in our system there was no detectable uptake of PLA-NP by neutrophils. This was unexpected since neutrophils often internalize circulating NP [46], but it is not unprecedented [22,45]. Neutrophils have been shown to phagocytose bacteria much more efficiently when presented on surfaces (*e.g.* after subcutaneous injection) than in the fluid phase (*e.g.* after intravenous injections) [47]. Yet, we could also not induce neutrophils to ingest PLA-NPs after sub-cutaneous injection (Data not shown).

During our investigation on the interactions of PLA-NP with macrophages, we could assess, using two different techniques (Flow cytometry and quantitative image analysis), a significant increase of PLA-NP internalized by macrophage from 30 min to 24 h following the injection. From this, we realized that macrophages continued to internalize PLA-NP despite the complete absence of detectable NP circulating in the blood flow (Fig. 4). We therefore investigated by live imaging how macrophages could continue to internalize PLA-NP at a time when no obvious pool of free NP was available. This analysis led us to unveil two different types of transfer of cytoplasmic material from endothelial cells to macrophages.

One of these processes involved the production of budding structures by endothelial cells that resemble microvesicles, which are then quickly internalized by adjacent macrophages (Fig. 6). Microvesicles are vesicles of around 100 nm to 1 μm that are generated through the budding outwards of domains from the plasma membrane and are involved in cell-cell communication [48–53]. Although no transfer of PLA-NP could be seen associated with this process, to our knowledge, our study is the first to provide live-observations of the genesis of microvesicles by endothelial cells and their subsequent internalization by adjacent macrophages in the zebrafish.

The second process involved the striking discovery of transfer of large PLA-NP-loaded cellular structures along with GFP-labelled cytoplasmic material from endothelial cells to macrophages (Fig. 5, Fig. S10), a phenomenon not previously described. This kind of transfer showed a consistent pattern with, first, a macrophage engaging contact with an endothelial cell for several minutes, followed by internalization of endothelial GFP-labelled cytoplasmic material containing PLA-NP loaded endocytic organelles. This was followed by the macrophage separating from the endothelial cell, which appeared unharmed. After the internalization, the fluorescence (GFP) from the endothelial material did not co-localize with the fluorescence (mCherry) from the macrophage cytosol, consistent with a phagocytic process internalizing the fragment of the endothelial cell (containing GFP and NP-containing vesicles) into a compartment of the endocytic pathway of the macrophage. This process involving NP transfer from endothelial cells to macrophages appears to be distinct from multiple known mechanisms involved in the transfer of material from one cell to another. As the transfer of NP we report involves the transfer of cytoplasmic fragments, we do not consider transcytosis as a plausible candidate.

Tunneling nanotubes involve the formation of cytoplasmic bridges that connect two cells and can be either long and narrow or short and thick, the latter being able to transfer organelles such as endosomes and mitochondria [54–56]. However, it is unlikely that tunneling nanotubes are related to our observations as they involve a direct connection and mixing of the cytoplasm of two adjacent cells.

We also considered the possibility that the NP transfer we observe might be related to apoptotic events. Apoptosis is a process of programmed cell death by which remnants of the dying cell can be internalized by macrophages through the uptake of apoptotic bodies, or *via* a process called efferocytosis [57,58]. Apoptotic bodies are large extracellular vesicles (1–5 μm) that contain an enclosed fraction of the apoptotic cells they originate from [59,60]. However, no apoptotic endothelial cells were observed in the region from which our videos were acquired and the donor endothelial cells appeared alive after the transfer. This is also consistent with the fact that at the early developmental stages we used, the vascular system of the zebrafish embryo is expanding, not regressing. Furthermore, we showed that the injection of PLA-NP triggers a transient and low induction of cell death that does not surpass the mechanical injury from a mock injection (Fig. 5). Thus, events related to the death of endothelial cell could hardly explain the increase of PLA-NP internalizations by macrophages that we monitored in the 24 h period after PLA-NP left the blood compartment.

We also envisaged the involvement of another described transfer mechanism, which shares similarities with the pattern we observed, especially the prolonged contact between the cells and the storage of the transferred cellular fragments apart from the cytosol. Trogocytosis is an event of partial phagocytosis that has been recently identified. Initially restricted to the nibbling of plasma membrane by T cells [61], since then, the definition of trogocytosis has being widened to include the partial phagocytosis of a donor cell, that remains alive in a healthy condition [62]. It has been reported that macrophages can perform trogocytosis [63], and in contrast to T lymphocytes, trogocytosed cellular fragments by macrophages usually end up being internalized

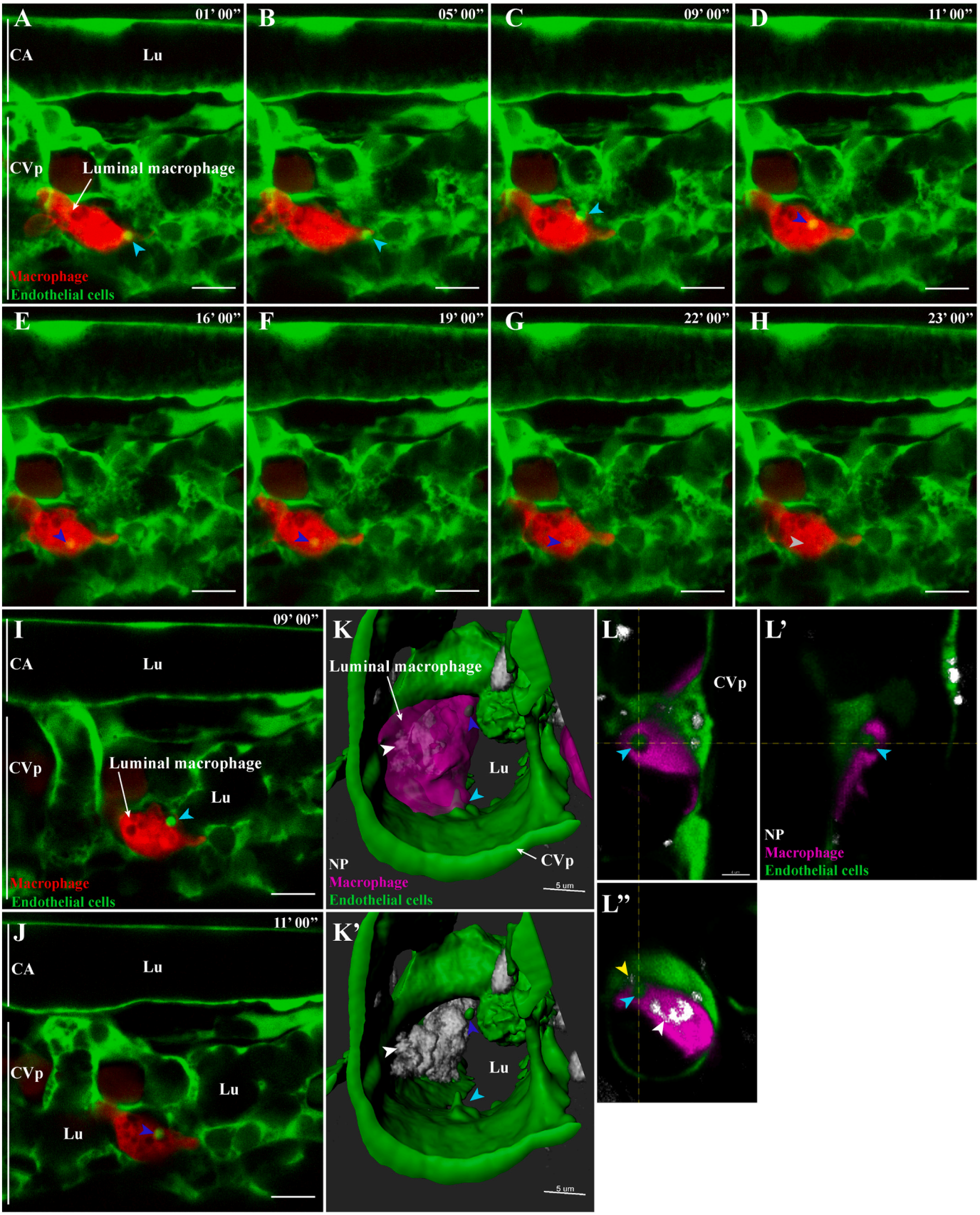

(caption on next page)

Fig. 6. Microvesicle-like transfer from endothelial cells to macrophages. Representative live-acquisitions of 3 dpf mpeg1:mCherry and fli:GFP double transgenic zebrafish, 30 min after the intravenous injection of far-red fluorescent PLA-NP and using a spinning-disk confocal microscope. The acquisitions have been made in the tail region, at the caudal vein plexus. Endothelial cells, macrophages and PLA-NP are highlighted in green, red and white, respectively. (A-B) At the start of the video (9 μm MIP), close to a macrophage residing in the bloodstream, an endothelial cell from the caudal vein plexus is forming a bright GFP+ microvesicle-like structure (cyan arrowhead). (C) Nine minutes later, the microvesicle-like structure is released from the endothelial cell (cyan arrowhead), it is then quickly internalized by the adjacent macrophage (D - blue arrowhead). Once internalized, the fluorescence of the microvesicle-like structure rapidly fades (E-G - blue arrowheads) to finally disappear 13 min after its internalization (H – grey arrowhead). Optical sections (1 μm) from (C) and (D), (I) highlights the contact between the GFP+ microvesicle and the plasma membrane of the macrophage (cyan arrowhead), while (J) emphasize its internalization inside a mCherry negative cellular compartment (blue arrowhead). (K-K′) A luminal macrophage, positive for PLA-NP (white arrowhead) and with a GFP+ cellular compartment (blue arrowhead) is wrapping around a budding microvesicle-like structure of an endothelial cell from the caudal vein plexus (cyan arrowhead). Fluorescence are represented as 3D reconstructions. (L-L") Orthogonal views from (K) reveal the presence of PLA-NP in close proximity to the budding-microvesicle-like structure (yellow arrowhead). Annotations: CA, caudal artery; CVp, caudal vein plexus and Lu, lumen. Scale bars: 10 um (A-J), 5 μm (K-K′) and 4 μm (L). (For interpretation of the references to colour in this figure legend, the reader is referred to the web version of this article.)

[64]. However, the trogocytosis of endothelial cells by macrophage has not been reported yet. The different discussed mechanisms are illustrated in Scheme 1.

The exchange of material from endothelial cell to macrophage we describe raises many questions regarding its biological significance. It is likely that this transfer of PLA-NP hijacks an existing mechanism that developed independently of the presence of foreign polymeric NP arriving *via* the blood stream. A plausible hypothesis could be a mechanism that would be involved in an immune surveillance *via* activation of antigen-presenting cells. Interestingly, a recent study on the internalization of silica nanoparticles (70 nm) by endothelial cells and macrophages did not observe any transfer [22]. Regarding its significance for the field of Nanomedicine, this exchange of NP from endothelial cells to associated macrophages represents a new type of biological interaction to be considered. It is likely to have important implications for the design of future NP treatment for vascular disease as it reveals macrophages as possible off-targets. However, it could also represent an interesting strategy to aim NP toward vascular-associated macrophages or to deliver compound to the microglia in the brain without having to disrupt the blood-brain barrier. This last prospect could also benefit anti-cancer treatment as Sofias et al. [65] showed the involvement of phagocytes in the accumulation of therapeutic nanoparticle from the blood to cancer area through a process called "phagocyte hitchhiking", something we also described in one of our recent study. [66]

4. Conclusion

In this study, we took advantage of the zebrafish model to deepen our understanding of the biological interaction and fate of safe-by-design surfactant-free PLA-NP after intravenous administration. Using live-imaging, flow-cytometry, light-microscopy and electron microscopy, we could follow in detail the interplays between PLA-NP, the endothelium and macrophages at the tissue, cellular and ultrastructural level. Our findings provide new insights into NP interaction with the vascular endothelium. The negatively-charged, surfactant-free PLA-NP were efficiently internalized by endothelial cells and macrophages. In contrast to other studies using anionic NP, our PLA-NP were distributed along the veins and arteries of the whole vasculature. A novelty of our approach was the encapsulation of hydrophobic gold particles into the matrix of PLA-NP to study their fate by electron microscopy, enabling analysis of their internalization by endothelial cells to their ongoing disassembly a week later.

In addition, our study is one of the first to evaluate the biodistribution of a surfactant-free NP system with a high quality of imaging and we believe that it will improve the understanding of how other surfactant-free NP can potentially behave *in vivo*.

Finally, a novel finding of our study is the existence of a new biological mechanism that allow cell-cell transfer of NP, from endothelial cells to macrophages. This could potentially be significant for the development of new NP therapy for vascular related disease and the targeting of macrophages. The precise mechanism and biological significance of this transfer of NP remain to be elucidated.

5. Material and methods

NP Preparation and Characterization.

Poly(lactic acid) nanoparticles were elaborated by nanoprecipitation as previously described [8,67,68] and were provided by Adjuvatis (i-particles®). Fluorophores were encapsulated using different fluorophore:PLA ratio: CellTrace BODIPY TR Methyl Ester ™ (0,02% - Life Technologies), BODIPY 500-510$_{C4,C9}$ ™ (0,04% - Life Technologies) and

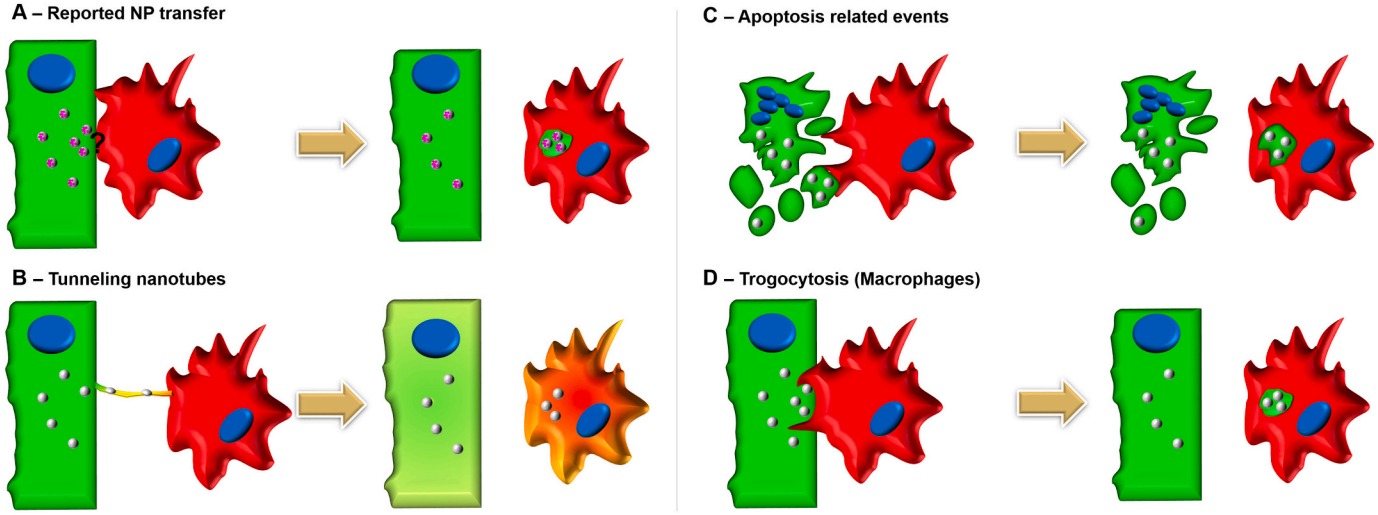

Scheme 1. Illustrations of the reported NP transfer and known Cell-Cell transfer mechanisms.

DY650-decylamide (0,10% - Dyomics GmbH). The characterization, by dynamic light scattering, of the size, as well as the size homogeneity of the different PLA-NP formulations were performed using a Zetasizer nanoS apparatus (Malvern Instrument, UK).

For the electron microscopy analysis, 6–7 nm hydrophobic colloidal gold particles (PlasmaChem) were encapsulated into the PLA-NP. For this, 20 mg of gold particles were dissolved in dichloroethane and poured in an acetone solution containing 90 mg of PLA before initiating the nanoprecipitation process. Solution were then kept for 18 h of storage in static mode to remove the pellet of any aggregated gold particles that had not been encapsulated. After characterization, the obtained PLA-NP(gold) displayed a mean diameter of 211,3 nm, a polydispersity index of 0,199 and an encapsulation yield of gold particles of 90%. As verified with electron microscopy (Fig. S4), essentially no free gold particles remained at the end of this process.

5.1. Animal care and ethic statement

Experiment were performed in accordance with the animal care guidelines, ethical standards and legislation of the European Union, France and Norway. Zebrafish embryos were reared and handled following such guidelines and laws. The experiments were conducted using wild-type AB/Tubingen zebrafish and genetically-modified strains *Tg(mpeg1:mCherry)gl23* [23], *Tg(fli1a:GFP)y1* [18] and *Tg(mpx:GFP)i114* [24].

5.2. Intravenous injection of PLA-NP into zebrafish embryos

Injection needles were produced using borosilicate capillaries (GC100T-10, Harvard Instruments) and a pipet puller (P-97, Sutter Instruments). The needles were loaded with an appropriate sample before being connected to an Eppendorf Femtojet Express pump and mounted onto a Narishige MN-153 micromanipulator that allowed movement in the x, y and z planes. Zebrafish embryos (3 dpf) were anesthetized using a solution of buffered tricaine (120 μg/mL) and 5 nL of PLA-NP (in PBS 1×) were injected into either the caudal vein plexus or the post-cardinal vein using a femtojet (Eppendorf) and a stereomicroscope (Leica DFC365FX). Unless specified, PLA-NP were concentrated at 0,5% (5 mg/mL), such injection represent a quantity of 1.10^6 to 5.10^6 nanoparticles.

To perform the experiment saturating scavenger endothelial cells with an anionic competitor, following the recommendations of Dr. Frederik Verweij [30], fish were administered intravenously 1 nL of dextran sulfate 500 KDa (Sigma), at either 3 mg/mL or 30 mg/mL, 2 h before the administration of PLA-NP. Only fish with regular blood flow were used for live-imaging at high-resolution.

5.3. Live-imaging

Following PLA-NP (0,5%) administration, stereomicroscope (Leica DFC365FX – 1.0× planapo lens) acquisitions were performed on 3 dpf zebrafish larvae that were maintained under anesthesia (buffered tricaine: 120 μg/mL) and placed onto an agarose support.

For the high-resolution live-imaging acquisitions, zebrafish larvae were maintained under anesthesia (buffered tricaine: 120 μg/mL), embedded in 1,5% low-melting agarose onto the coverslip of a round petridish. Images/videos were then acquired at 28 °C using the Zyla camera of a Dragonfly spinning disk confocal microscope (Andor), 40 μm pinholes and a 60×/1.2-water immersion objective. Acquisitions were performed using the Fusion software, while image/video analysis was made using both IMARIS and ImageJ softwares.

5.4. Toxicity and cell death assays

5.4.1. Toxicity

Zebrafish larvae (3 dpf) were injected as described above with 5 nL of either green, red or far-red fluorescent PLA-NP (0,5%), 20 zebrafish larvae were used per fluorescent PLA-NP. Injected fish were then individually placed into the wells of 24 wells-plates with 2 mL of embryo water per fish. Following 24 h at 28 °C, the number of death was counted, taking into account lethal and sub-lethal phenotypes such as no heart-beat, oedema, malformation and weak blood flow.

5.4.2. Cell death assay

Zebrafish larvae (3 dpf) were injected as described above with 5 nL of either green, red or far-red fluorescent PLA-NP (0,5%), PBS 1× or DMSO 80%. At 30 min and 24 h post-injection, fish were incubated in a solution of acridine orange 10 μg/mL (Sigma) for 20 min. After 3 rinses in embryo water, zebrafish larvae were anesthetized with buffered tricaine (120 μg/mL) and placed onto an agarose support to acquire the total fluorescence associated to acridine orange with a stereomicroscope (Leica DFC365FX – 1.0× planapo lens).

5.5. Histology – light microscopy

Zebrafish larvae were injected with fluorescent PLA-NP (0,5%) as previously described and were euthanized with an overdose of buffered tricaine 30 min, 4 h and 24 h later. They were then immediatly fixed with a solution of methanol-free 4% PFA in hepes buffer 60 mM pH 7,4 for 24 h at room temperature, cryoprotected in a solution of sucrose 30% for 24 h, embedded in Tissue-Tek O.C.T. Compound (Sakura Finetek USA), flash frozen in isopentane, and sectioned using a CM1950 cryostat (Leica). The resulting 30-μm cryosections were recovered on superfrost plus slide (Thermofischer). Obtained sections were counterstained with a solution of phalloidin conjugated with either Dylight-633 or Alexa-647 (3 U/mL - Life technologies), and DAPI (5 μg/mL - Sigma). Sections were then mounted with prolong-glass mounting medium (Life technologies) and cured for 24 h to reach a theoretical refractive index of 1,52. Acquisitions were made using the Zyla camera of a Dragonfly spinning disk confocal microscope (Andor), 40 μm pinholes and a 60×/1.4-oil immersion objective. Acquisitions were performed using features from the Fusion software, while image analysis was made using both IMARIS and ImageJ softwares. Some acquisitions were made using a SP5 confocal microscope (Leica).

5.6. Histology – electron microscopy

Zebrafish larvae were injected with PLA-NP(gold) as previously described and euthanized with an overdose of buffered tricaine 10 min, 30 min, 4 h, 24 h, 72 h, 96 h and one week post-injection. They were then immediately fixed in a solution of glutaraldehyde (1,5%) and PFA (1%) buffered with cacodylate 0,1% pH: 7,4 overnight at 4 °C. Following rinses with a solution of cacodylate 0,1 M / sucrose 8%, samples were incubated 1 h with osmium tetraoxyde. Samples were then rinsed with distilled water, progressively dehydrated with ethanol solutions (30–100%) and embedded in Epon at 60C degree for several days. Following complete polymerization, 60 nm ultrathin sections were realized and mounted onto copper grids. Finally, acquisitions without additional contrast were made using an transmission electron microscope MET PHILIPS CM120 with GATAN Orius200 2Kx2K camera with a maximum resolution of 0,34 nm (Centre Technologique des Microstructures, Lyon, France). Image analysis was made using ImageJ softwares.

5.7. Quantification of PLA-NP internalization by macrophages

5.7.1. Flow cytometry

Transgenic mpeg1:mCherry zebrafish (3 dpf) were intravenously injected with less concentrated green fluorescent PLA-NP (0,25%) to reduce the risk of false-positive event detection due to the presence of non-internalized PLA-NP 10 min post-injection. Fish were euthanized by overdose of buffered tricaine at 4 °C 10 min, 30 min, 2 h, 4 h and 24 h post-injection. For each time-point, 10 larvae per replicate were

injected. Samples were chopped in fine pieces using microscissors and incubated in a solution of versene water (Life Technologies) complemented with trypsine (2 g/L), under constant steering. Samples were then placed onto ice, complemented with fetal calf serum (FCS) to inhibite the digestion and processed through 40 μm cell strainers (Thermofisher). Resulting cell suspensions were centrifugated (400 g, 8 min, 4C degree) and resuspended in PBS 1× with 4% FCS. To allow the exclusion of dead cells, samples were complemented with DAPI (2,5 μg/mL) right before the acquisitions by LSRII (Bioscience) flow cytometer. Acquisitions were analyzed using the FlowJo v7.6.5 software.

5.7.2. Automated quantification

The measuring of macrophage uptake has been previously described in a recent publication [31] using a Fiji MACRO which was also used here.

For this experiment, the zebrafish strain *Tg(mpeg1:mCherry)gl23* [23] having red fluorescently labelled macrophages was used. Five nanoliters of green fluorescent PLA NP were injected in the zebrafish posterior cardinal vein and, by using a Leica stereomicroscope DFC365FX (1.0× planapo lens), images of the whole zebrafish (30×) or the caudal region were taken (120×) at 30 min and 24 h after injection. Using the program Fiji, the fluorescence of the pixels (expressed as RawIntDen) relative to PLA NP that were found in Macrophage positive selection was normalized by the overall fluorescence (also expressed as RawIntDen) and multiplied by 100. The formula can be expressed as follows:

$$\text{Macrophage accumulation } (30\ min \text{ or } 24\text{ h}) = \frac{Raw\ int\ Den\ Macrophages\ (30\ min, 24h)}{Raw\ Int\ Den\ Whole\ zebrafish\ (30\ min, 24\ h)}\ X\ 100$$

5.8. Statistical analysis

Statistical analyses were performed using GraphPad Prism 8.0.1. Normality of samples was tested using Agostino and Pearson omnibus normality test. For the quantification of PLA-NP internalization by macrophages, populations did not display a normal distribution so a non-parametric one-tailed Mann-Whitney test was carried. For the cell death assay, all populations were displaying a normal distribution, thus we carried a one-way ANOVA coupled with Bonferroni's multiple comparisons *post hoc* analysis. Significance level is indicated as $*p < .05$, $**p < .01$, $***p < .001$, $****p < .0001$.

Supplementary data to this article can be found online at https://doi.org/10.1016/j.jconrel.2021.01.006.

Supplementary material

Declaration of Competing Interest

BV and CP declare financial interest in Adjuvatis. The remaining authors declare no competing financial interest.

Acknowledgement

We thank the Norwegian Research Counsil for funding (FRIMEDBIO-No 144642). This work was also supported by the ANR project Fish-RNAVax (ANR-16-CE20-0002-01 and ANR-16-CE20-0002-03) and by Euronanomed III (Flunanoair).

We thank the PRECI fish facility (L.Bernard and R.Renard), the AniRA-Cytométrie platform (T.Andrieu and S.Dussurgey), the PLATIM-Microscopy plateform of SFR Biosciences Gerland-Lyon Sud (UMS3444/US8). We would also like to thank the Primatiss histology plateform (C.Lethias and N. El Kholti) from IBCP, the CTμ (Centre Technologique des Microstructures) electron microscopy plateform from UCBL, the EM-lab from the university of Oslo (N.Roos and head engineers), the fish facility (AC.Tavara and J.Santana) of NCMM, the Oslo NorMIC imaging plateform (O.Bakke, F.Skjeldal and L.Haugen). We address a special thanks to E.Delaune, S.Essayar, D.Ficheux, V. Bjørnestad, F.Verweij, D.Frei and B.Mathiesen for their advices and assistance.

References

[1] K. Park, Facing the truth about nanotechnology in drug delivery, ACS Nano 7 (2013) 7442–7447, https://doi.org/10.1021/nn404501g.
[2] N. Sharma, P. Madan, S. Lin, Effect of process and formulation variables on the preparation of parenteral paclitaxel-loaded biodegradable polymeric nanoparticles: a co-surfactant study, Asian J. Pharm. Sci. 11 (2016) 404–416, https://doi.org/10.1016/j.ajps.2015.09.004.
[3] P.J. Kennedy, I. Perreira, D. Ferreira, M. Nestor, C. Oliveira, P.L. Granja, B. Sarmento, Impact of surfactants on the target recognition of fab-conjugated PLGA nanoparticles, Eur. J. Pharm. Biopharm. 127 (2018) 366–370, https://doi.org/10.1016/J.EJPB.2018.03.005.
[4] L. Araujo, R. Löbenberg, J. Kreuter, Influence of the surfactant concentration on the body distribution of nanoparticles, J. Drug Target. 6 (1999) 373–385, https://doi.org/10.3109/10611869908996844.
[5] S.K. Sahoo, J. Panyam, S. Prabha, V. Labhasetwar, Residual polyvinyl alcohol associated with poly (d,l-lactide-co-glycolide) nanoparticles affects their physical properties and cellular uptake, J. Control. Release 82 (2002) 105–114, https://doi.org/10.1016/S0168-3659(02)00127-X.
[6] N. Grabowski, H. Hillaireau, J. Vergnaud, N. Tsapis, M. Pallardy, S. Kerdine-Römer, E. Fattal, Surface coating mediates the toxicity of polymeric nanoparticles towards human-like macrophages, Int. J. Pharm. 482 (2015) 75–83, https://doi.org/10.1016/j.ijpharm.2014.11.042.
[7] M. Lamrayah, F. Charriaud, S. Hu, S. Megy, R. Terreux, B. Verrier, Molecular modelling of TLR agonist Pam3CSK4 entrapment in PLA nanoparticles as a tool to explain loading efficiency and functionality, Int. J. Pharm. 568 (2019), https://doi.org/10.1016/j.ijpharm.2019.118569.
[8] C. Primard, N. Rochereau, E. Luciani, C. Genin, T. Delair, S. Paul, B. Verrier, Traffic of poly(lactic acid) nanoparticulate vaccine vehicle from intestinal mucus to sub-epithelial immune competent cells, Biomaterials. 31 (2010) 6060–6068, https://doi.org/10.1016/j.biomaterials.2010.04.021.
[9] K. Park, Drug delivery research: the invention cycle, Mol. Pharm. 13 (2016) 2143–2147, https://doi.org/10.1021/acs.molpharmaceut.6b00015.
[10] M. Barz, Complexity and simplification in the development of nanomedicines, Nanomedicine. 10 (2015) 3093–3097, https://doi.org/10.2217/nnm.15.146.
[11] V. Pavot, N. Climent, N. Rochereau, F. Garcia, C. Genin, G. Tiraby, F. Vernejoul, E. Perouzel, T. Lioux, B. Verrier, S. Paul, Directing vaccine immune responses to mucosa by nanosized particulate carriers encapsulating NOD ligands, Biomaterials. 75 (2016) 327–339, https://doi.org/10.1016/j.biomaterials.2015.10.034.
[12] A.-L. Coolen, C. Lacroix, P. Mercier-Gouy, E. Delaune, C. Monge, J.-Y. Exposito, B. Verrier, Poly(lactic acid) nanoparticles and cell-penetrating peptide potentiate mRNA-based vaccine expression in dendritic cells triggering their activation, Biomaterials 195 (2019) 23–37, https://doi.org/10.1016/J.BIOMATERIALS.2018.12.019.
[13] F. Fenaroli, U. Repnik, Y. Xu, K. Johann, S. Van Herck, P. Dey, F.M. Skjeldal, D. M. Frei, S. Bagherifam, A. Kocere, R. Haag, B.G. De Geest, M. Barz, D.G. Russell, G. Griffiths, Enhanced permeability and retention-like extravasation of nanoparticles from the vasculature into tuberculosis granulomas in zebrafish and mouse models, ACS Nano 12 (2018) 8646–8661, https://doi.org/10.1021/acsnano.8b04433.
[14] F. Fenaroli, D. Westmoreland, J. Benjaminsen, T. Kolstad, F.M. Skjeldal, A. H. Meijer, M. van der Vaart, L. Ulanova, N. Roos, B. Nyström, J. Hildahl, G. Griffiths, Nanoparticles as drug delivery system against tuberculosis in zebrafish embryos: direct visualization and treatment, ACS Nano 8 (2014) 7014–7026, https://doi.org/10.1021/nn5019126.
[15] J. Rességuier, E. Delaune, A.-L. Coolen, J.-P. Levraud, P. Boudinot, D. Le Guellec, B. Verrier, Specific and efficient uptake of surfactant-free poly(lactic acid) nanovaccine vehicles by mucosal dendritic cells in adult zebrafish after bath immersion, Front. Immunol. 8 (2017) 190, https://doi.org/10.3389/fimmu.2017.00190.
[16] L. Treuel, K.A. Eslahian, D. Docter, T. Lang, R. Zellner, K. Nienhaus, G.U. Nienhaus, R.H. Stauber, M. Maskos, Physicochemical characterization of nanoparticles and their behavior in the biological environment, Phys, Chem. Chem. Phys. Phys. Chem. Chem. Phys. 16 (2014) 15053–15067, https://doi.org/10.1039/c4cp00058g.
[17] L. Evensen, P.L. Johansen, G. Koster, K. Zhu, L. Herfindal, M. Speth, F. Fenaroli, J. Hildahl, S. Bagherifam, C. Tulotta, L. Prasmickaite, G.M. Mælandsmo, E. Snaar-Jagalska, G. Griffiths, Zebrafish as a model system for characterization of nanoparticles against cancer, Nanoscale. 8 (2016) 862–877, https://doi.org/10.1039/C5NR07289A.
[18] N.D. Lawson, B.M. Weinstein, In Vivo imaging of embryonic vascular development using transgenic zebrafish, Dev. Biol. 248 (2002) 307–318, https://doi.org/10.1006/dbio.2002.0711.
[19] F. Campbell, F.L. Bos, S. Sieber, G. Arias-Alpizar, B.E. Koch, J. Huwyler, A. Kros, J. Bussmann, Directing nanoparticle biodistribution through evasion and exploitation of Stab2-dependent nanoparticle uptake, ACS Nano 12 (2018) 2138–2150, https://doi.org/10.1021/acsnano.7b06995.
[20] X.-Y. Jiang, C.D. Sarsons, M.J. Gomez-Garcia, D.T. Cramb, K.D. Rinker, S.J. Childs, Quantum dot interactions and flow effects in angiogenic zebrafish (Danio rerio) vessels and human endothelial cells, Nanomed. Nanotechnol. Biol. Med. 13 (2017) 999–1010, https://doi.org/10.1016/J.NANO.2016.12.008.

[21] L.Q. Chen, C.Z. Ding, J. Ling, Intensive epidermal adsorption and specific venous deposition of carboxyl quantum dots in zebrafish early-life stages, Chemosphere. 184 (2017) 44–52, https://doi.org/10.1016/J.CHEMOSPHERE.2017.05.173.
[22] Y. Hayashi, M. Takamiya, P.B. Jensen, I. Ojea-Jiménez, H. Claude, C. Antony, K. Kjaer-Sorensen, C. Grabher, T. Boesen, D. Gilliland, C. Oxvig, U. Strähle, C. Weiss, Differential nanoparticle sequestration by macrophages and scavenger endothelial cells visualized in vivo in real-time and at ultrastructural resolution, ACS Nano (2020), https://doi.org/10.1021/acsnano.9b07233.
[23] F. Ellett, L. Pase, J.W. Hayman, A. Andrianopoulos, G.J. Lieschke, mpeg1 promoter transgenes direct macrophage-lineage expression in zebrafish, Blood. 117 (2011) e49–e56, https://doi.org/10.1182/blood-2010-10-314120.
[24] S.A. Renshaw, C.A. Loynes, D.M.I. Trushell, S. Elworthy, P.W. Ingham, M.K. B. Whyte, A transgenic zebrafish model of neutrophilic inflammation, Blood. 108 (2006) 3976–3978, https://doi.org/10.1182/blood-2006-05-024075.
[25] R. Kalluru, F. Fenaroli, D. Westmoreland, L. Ulanova, A. Maleki, N. Roos, M. Paulsen Madsen, G. Koster, W. Egge-Jacobsen, S. Wilson, H. Roberg-Larsen, G. K. Khuller, A. Singh, B. Nyström, G. Griffiths, Poly(lactide-co-glycolide)-rifampicin nanoparticles efficiently clear Mycobacterium bovis BCG infection in macrophages and remain membrane-bound in phago-lysosomes, J. Cell Sci. 126 (2013) 3043–3054, https://doi.org/10.1242/jcs.121814.
[26] J.-Y. Jeong, H.-B. Kwon, J.-C. Ahn, D. Kang, S.-H. Kwon, J.A. Park, K.-W. Kim, Functional and developmental analysis of the blood–brain barrier in zebrafish, Brain Res. Bull. 75 (2008) 619–628, https://doi.org/10.1016/J.BRAINRESBULL.2007.10.043.
[27] A.G. Kramer-Zucker, S. Wiessner, A.M. Jensen, I.A. Drummond, Organization of the pronephric filtration apparatus in zebrafish requires Nephrin, Podocin and the FERM domain protein mosaic eyes, Dev. Biol. 285 (2005) 316–329, https://doi.org/10.1016/J.YDBIO.2005.06.038.
[28] M. Longmire, P.L. Choyke, H. Kobayashi, Clearance properties of nano-sized particles and molecules as imaging agents: considerations and caveats, Nanomedicine (Lond). 3 (2008) 703–717, https://doi.org/10.2217/17435889.3.5.703.
[29] H.W. Ferguson, M.J. Claxton, R.D. Moccia, E.J. Wilkie, The quantitative clearance of bacteria from the bloodstream of rainbow trout (Salmo gairdneri), Vet. Pathol. 19 (1982) 687–699. http://www.ncbi.nlm.nih.gov/pubmed/7147628 (accessed December 8, 2015).
[30] F.J. Verweij, V. Hyenne, G. Van Niel, J.G. Goetz, Extracellular vesicles: catching the light in Zebrafish, Trends Cell Biol. 29 (2019) 770–776, https://doi.org/10.1016/j.tcb.2019.07.007.
[31] N.K. Dal, A. Kocere, J. Wohlmann, S. Van Herck, T.A. Bauer, J. Resseguier, S. Bagherifam, H. Hyldmo, M. Barz, B.G. De Geest, F. Fenaroli, Zebrafish embryos allow prediction of nanoparticle circulation times in mice and facilitate quantification of nanoparticle–cell interactions, Small 16 (2020) 1906719, https://doi.org/10.1002/smll.201906719.
[32] Y.-L. Hu, W. Qi, F. Han, J.-Z. Shao, J.-Q. Gao, Toxicity evaluation of biodegradable chitosan nanoparticles using a zebrafish embryo model, Int. J. Nanomed. 6 (2011) 3351–3359, https://doi.org/10.2147/IJN.S25853.
[33] M. Furutani-Seiki, Y.J. Jiang, M. Brand, C.P. Heisenberg, C. Houart, D. Beuchle, F. J. van Eeden, M. Granato, P. Haffter, M. Hammerschmidt, D.A. Kane, R.N. Kelsh, M.C. Mullins, J. Odenthal, C. Nüsslein-Volhard, Neural degeneration mutants in the zebrafish, *Danio rerio*, Development. 123 (1996) 229–239. http://www.ncbi.nlm.nih.gov/pubmed/9007243 (accessed July 15, 2019).
[34] S. Sieber, P. Grossen, J. Bussmann, F. Campbell, A. Kros, D. Witzigmann, J. Huwyler, Zebrafish as a preclinical in vivo screening model for nanomedicines, Adv. Drug Deliv. Rev. (2019), https://doi.org/10.1016/J.ADDR.2019.01.001.
[35] F.J. Verweij, C. Revenu, G. Arras, F. Dingli, D. Loew, D.M. Pegtel, G. Follain, G. Allio, J.G. Goetz, P. Zimmermann, P. Herbomel, F. Del Bene, G. Raposo, G. van Niel, Live tracking of inter-organ communication by endogenous exosomes in vivo, Dev. Cell. 1 (2019), https://doi.org/10.1016/J.DEVCEL.2019.01.004, 573-589.e4.
[36] V. Hyenne, S. Ghoroghi, M. Collot, J. Bons, G. Follain, S. Harlepp, B. Mary, J. Bauer, L. Mercier, I. Busnelli, O. Lefebvre, N. Fekonja, M.J. Garcia-Leon, P. Machado, F. Delalande, A.A. López, S.G. Silva, F.J. Verweij, G. van Niel, F. Djouad, H. Peinado, C. Carapito, A.S. Klymchenko, J.G. Goetz, Studying the fate of tumor extracellular vesicles at high spatiotemporal resolution using the zebrafish embryo, Dev. Cell 48 (2019), https://doi.org/10.1016/J.DEVCEL.2019.01.014, 554-572.e7.
[37] S.H.C. Askes, N. Bossert, J. Bussmann, V.S. Talens, M.S. Meijer, R.E. Kieltyka, A. Kros, S. Bonnet, D. Heinrich, Dynamics of dual-fluorescent polymersomes with durable integrity in living cancer cells and zebrafish embryos, Biomaterials. 168 (2018) 54–63, https://doi.org/10.1016/J.BIOMATERIALS.2018.03.037.
[38] K.K. Sørensen, P. McCourt, T. Berg, C. Crossley, D. Le Couteur, K. Wake, B. Smedsrød, The scavenger endothelial cell: a new player in homeostasis and immunity, Am. J. Physiol. Regul. Integr. Comp. Physiol. 303 (2012) R1217–R1230, https://doi.org/10.1152/ajpregu.00686.2011.
[39] R. Kjeken, S.A. Mousavi, A. Brech, T. Gjøen, T. Berg, Fluid phase endocytosis of [125 I]iodixanol in rat liver parenchymal, endothelial and Kupffer cells, Cell Tissue Res. 304 (2001) 221–230, https://doi.org/10.1007/s004410100348.
[40] K. Ohtani, Y. Suzuki, S. Eda, T. Kawai, T. Kase, H. Keshi, Y. Sakai, A. Fukuoh, T. Sakamoto, H. Itabe, T. Suzutani, M. Ogasawara, I. Yoshida, N. Wakamiya, The membrane-type collectin CL-P1 is a scavenger receptor on vascular endothelial cells, J. Biol. Chem. 276 (2001) 44222–44228, https://doi.org/10.1074/jbc.M103942200.
[41] J.S. Suk, Q. Xu, N. Kim, J. Hanes, L.M. Ensign, PEGylation as a strategy for improving nanoparticle-based drug and gene delivery, Adv. Drug Deliv. Rev. 99 (2016) 28–51, https://doi.org/10.1016/j.addr.2015.09.012.
[42] H. Tanisaka, S. Kizaka-Kondoh, A. Makino, S. Tanaka, M. Hiraoka, S. Kimura, Near-infrared fluorescent Labeled Peptosome for application to cancer imaging, Bioconjug. Chem. 19 (2008) 109–117, https://doi.org/10.1021/bc7001665.
[43] K. Klinker, M. Barz, Polypept(o)ides: hybrid systems based on polypeptides and polypeptoids, Macromol. Rapid Commun. 36 (2015) 1943–1957, https://doi.org/10.1002/marc.201500403.
[44] S. Sieber, P. Grossen, P. Uhl, P. Detampel, W. Mier, D. Witzigmann, J. Huwyler, Zebrafish as a predictive screening model to assess macrophage clearance of liposomes in vivo, Nanomed. Nanotechnol. Biol. Med. 17 (2019) 82–93, https://doi.org/10.1016/J.NANO.2018.11.017.
[45] L. Rizzello, J.D. Robertson, P.M. Elks, A. Poma, N. Daneshpour, T.K. Prajsnar, D. Evangelopoulos, J.O. Canseco, S. Yona, H.M. Marriott, D.H. Dockrell, S.J. Foster, B. De Geest, S. De Koker, T. Mchugh, S.A. Renshaw, G. Battaglia, Targeting mononuclear phagocytes for eradicating intracellular parasites, 2017, https://doi.org/10.1101/119297.
[46] J.D. Robertson, J.R. Ward, M. Avila-Olias, G. Battaglia, S.A. Renshaw, Targeting neutrophilic inflammation using polymersome-mediated cellular delivery, J. Immunol. 198 (2017) 3596–3604, https://doi.org/10.4049/JIMMUNOL.1601901.
[47] E. Colucci-Guyon, J.Y. Tinevez, S.A. Renshaw, P. Herbomel, Strategies of professional phagocytes in vivo: unlike macrophages, neutrophils engulf only surface-associated microbes, J. Cell Sci. 124 (2011) 3053–3059, https://doi.org/10.1242/jcs.082792.
[48] J. Ratajczak, M. Wysoczynski, F. Hayek, A. Janowska-Wieczorek, M.Z. Ratajczak, Membrane-derived microvesicles: important and underappreciated mediators of cell-to-cell communication, Leukemia. 20 (2006) 1487–1495, https://doi.org/10.1038/sj.leu.2404296.
[49] F. Jansen, Q. Li, A. Pfeifer, N. Werner, Endothelial- and immune cell-derived extracellular vesicles in the regulation of cardiovascular health and disease, JACC. Basic Transl. Sci. 2 (2017) 790–807, https://doi.org/10.1016/j.jacbts.2017.08.004.
[50] M. Colombo, G. Raposo, C. Théry, Biogenesis, Secretion, and Intercellular interactions of exosomes and other extracellular vesicles, Annu. Rev. Cell Dev. Biol. 30 (2014) 255–289. doi:https://doi.org/10.1146/annurev-cellbio-101512-122326.
[51] G. Camussi, M.C. Deregibus, S. Bruno, V. Cantaluppi, L. Biancone, Exosomes/microvesicles as a mechanism of cell-to-cell communication, Kidney Int. 78 (2010) 838–848, https://doi.org/10.1038/KI.2010.278.
[52] C. Hromada, S. Mühleder, J. Grillari, H. Redl, W. Holnthoner, Endothelial extracellular vesicles—promises and challenges, Front. Physiol. 8 (2017) 275, https://doi.org/10.3389/fphys.2017.00275.
[53] A. Słomka, S.K. Urban, V. Lukacs-Kornek, E. Żekanowska, M. Kornek, Large extracellular vesicles: have we found the holy grail of inflammation? Front. Immunol. 9 (2018) 2723, https://doi.org/10.3389/fimmu.2018.02723.
[54] A. Sartori-Rupp, D. Cordero Cervantes, A. Pepe, K. Gousset, E. Delage, S. Corroyer-Dulmont, C. Schmitt, J. Krijnse-Locker, C. Zurzolo, Correlative cryo-electron microscopy reveals the structure of TNTs in neuronal cells, Nat. Commun. 10 (2019) 342, https://doi.org/10.1038/s41467-018-08178-7.
[55] S. Abounit, C. Zurzolo, Wiring through tunneling nanotubes–from electrical signals to organelle transfer, J. Cell Sci. 125 (2012) 1089–1098, https://doi.org/10.1242/jcs.083279.
[56] D.M. Frei, E. Hodneland, I. Rios-Mondragon, A. Burtey, B. Neumann, J. Bulkescher, J. Schölermann, R. Pepperkok, H.-H. Gerdes, T. Kögel, Novel microscopy-based screening method reveals regulators of contact-dependent intercellular transfer, Sci. Rep. 5 (2015) 12879, https://doi.org/10.1038/srep12879.
[57] R.W. Vandivier, P.M. Henson, I.S. Douglas, Burying the dead: the impact of failed apoptotic cell removal (efferocytosis) on chronic inflammatory lung disease, Chest. 129 (2006) 1673–1682, https://doi.org/10.1378/CHEST.129.6.1673.
[58] S.J. Gardai, K.A. McPhillips, S.C. Frasch, W.J. Janssen, A. Starefeldt, J.E. Murphy-Ullrich, D.L. Bratton, P.-A. Oldenborg, M. Michalak, P.M. Henson, Cell-surface Calreticulin initiates clearance of viable or apoptotic cells through trans-activation of LRP on the phagocyte, Cell. 123 (2005) 321–334, https://doi.org/10.1016/J.CELL.2005.08.032.
[59] L. Jiang, S. Paone, S. Caruso, G.K. Atkin-Smith, T.K. Phan, M.D. Hulett, I.K.H. Poon, Determining the contents and cell origins of apoptotic bodies by flow cytometry, Sci. Rep. 7 (2017) 14444, https://doi.org/10.1038/s41598-017-14305-z.
[60] J.C. Akers, D. Gonda, R. Kim, B.S. Carter, C.C. Chen, Biogenesis of extracellular vesicles (EV): exosomes, microvesicles, retrovirus-like vesicles, and apoptotic bodies, J. Neuro-Oncol. 113 (2013) 1–11, https://doi.org/10.1007/s11060-013-1084-8.
[61] E. Joly, D. Hudrisier, What is trogocytosis and what is its purpose? Nat. Immunol. 4 (2003) 815, https://doi.org/10.1038/ni0903-815.
[62] F. Zeng, A.E. Morelli, Extracellular vesicle-mediated MHC cross-dressing in immune homeostasis, transplantation, infectious diseases, and cancer, Semin. Immunopathol. 40 (2018) 477–490, https://doi.org/10.1007/s00281-018-0679-8.
[63] A.K. Sárvári, Q.-M. Doan-Xuan, Z. Bacsó, I. Csomós, Z. Balajthy, L. Fésüs, Interaction of differentiated human adipocytes with macrophages leads to trogocytosis and selective IL-6 secretion, Cell Death Dis. 6 (2015) e1613, https://doi.org/10.1038/cddis.2014.579.
[64] T. Pham, P. Mero, J.W. Booth, Dynamics of macrophage trogocytosis of rituximab-coated B cells, PLoS One 6 (2011) e14498, https://doi.org/10.1371/journal.pone.0014498.
[65] A.M. Sofias, Y.C. Toner, A.E. Meerwaldt, M.M.T. van Leent, G. Soultanidis, M. Elschot, H. Gonai, K. Grendstad, Å. Flobak, U. Neckmann, C. Wolowczyk, E. L. Fisher, T. Reiner, C.L. Davies, G. Bjørkøy, A.J.P. Teunissen, J. Ochando, C. Pérez-Medina, W.J.M. Mulder, S. Hak, Tumor targeting by αvβ3-integrin-specific lipid

nanoparticles occurs via phagocyte hitchhiking, ACS Nano 14 (2020) 7832–7846, https://doi.org/10.1021/acsnano.9b08693.

[66] A. Kocere, J. Resseguier, J. Wohlmann, F.M. Skjeldal, S. Khan, M. Speth, N.J.K. Dal, M.Y.W. Ng, N. Alonso-Rodriguez, E. Scarpa, L. Rizzello, G. Battaglia, G. Griffiths, F. Fenaroli, Real-time imaging of polymersome nanoparticles in zebrafish embryos engrafted with melanoma cancer cells: Localization, toxicity and treatment analysis, EBioMedicine 58 (2020) 102902, https://doi.org/10.1016/j.ebiom.2020.102902.

[67] D. Lamalle-Bernard, S. Munier, C. Compagnon, M.-H. Charles, V.S. Kalyanaraman, T. Delair, B. Verrier, Y. Ataman-Onal, Coadsorption of HIV-1 p24 and gp120 proteins to surfactant-free anionic PLA nanoparticles preserves antigenicity and immunogenicity, J. Control. Release 115 (2006) 57–67, https://doi.org/10.1016/j.jconrel.2006.07.006.

[68] V. Pavot, N. Rochereau, C. Primard, C. Genin, E. Perouzel, T. Lioux, S. Paul, B. Verrier, Encapsulation of Nod1 and Nod2 receptor ligands into poly(lactic acid) nanoparticles potentiates their immune properties, J. Control. Release 167 (2013) 60–67, https://doi.org/10.1016/j.jconrel.2013.01.015.